Modulation of calcineurin activity in *Aspergillus nidulans*: the roles of high magnesium concentrations and of transcriptional factor CrzA.

Running title: Roles of magnesium and CrzA in calcineurin signaling

Authors: Maria-Tsampika Manoli and Eduardo A. Espeso*.

Contact information: Department of Cellular and Molecular Biology, Centro de Investigaciones Biológicas (CIB), CSIC. Ramiro de Maeztu, 9. Madrid 28040. Spain

email: eespeso@cib.csic.es

*corresponding author

Keywords: Signaling, Calcineurin, alkaline pH, calcium sensitivity, filamentous fungus

Acknowledgments:

To Ane Markina for her seminal work on the construct of null *midA* and *cchA* strains. To Gustavo Goldman for sharing the *cnaB2* mutant. Thanks to Vivian de los Rios and Francisco Garcia from the CIB's Proteomic and Genomic facilities for their help with the phosphoproteomic analysis. To unknown reviewers and to Steve Harris for their helpful suggestions. This work was supported by grants BFU2012-33142 and BFU2015-66806-R from the MINECO/FEDER/EU, Spain, to E.A.E.

Author Contributions:

EAE and M-TM conceived and designed the experimental work. M-TM performed the experiments and both authors interpreted the data; EAE and M-TM wrote the manuscript

Title: Modulation of calcineurin activity in *Aspergillus nidulans*: the roles of high magnesium concentrations and of transcriptional factor CrzA

Summary

A proper response to elevated extracellular calcium levels helps to most organisms to keep this secondary messenger under strict control, thereby preventing inadequate activation or inhibition of many regulatory activities into cells. In fungi, the calcineurin responsive zinc-finger Crz1/CrzA transcription factor transduces calcium signaling to gene expression. In *Aspergillus nidulans*, absence of CrzA activity leads to alkaline pH sensitivity and loss of tolerance to high levels of extracellular calcium. Disruption of calcium uptake mechanisms or the presence of high levels of Mg^{2+} partially suppresses this calcium-sensitive phenotype of null *crzA* strain. The effects of Mg^{2+} on CrzA phosphorylation and perturbations that reduce calcineurin phosphatase activity on CrzA demonstrate that the calcium sensitive phenotype of null *crzA* strain is a consequence of up-regulated calcineurin activity under calcium-induced conditions.

Keywords: Signaling, Calcineurin, alkaline pH, calcium sensitivity, filamentous fungus

Introduction

Calcium and magnesium are central cations for cell survival because they participate in the regulation of numerous processes in either prokaryotes or eukaryotes. Accordingly, to their importance, their intracellular concentrations are tightly regulated. Environments with abundant Ca^{2+} or Mg^{2+} can challenge homeostatic mechanisms (Wolf and Trapani, 2008) (Cunningham, 2005). On the other hand, limitation of Ca^{2+} and Mg^{2+} supply can also constrain microbial growth. Both cations can enter the cell through different transport mechanisms and, due to the importance of these cations, it must exist a feedback control system in order to regulate the levels of free cytosolic Ca^{2+} and Mg^{2+}. Regulation of the cytosolic free-ionized Mg^{2+} concentration is likely achieved by three major mechanisms: control of uptake systems, efflux from the cell and sequestration within organelles (Grubbs, 2002). Levels of intracellular calcium are carefully regulated to enable a stable cytosolic concentration of 50-200 nM (Aiello *et al.*, 2002). From fungi to metazoans, the elevation of cytosolic calcium levels sequentially activates a signaling cascade based on two calcium binding proteins, calmodulin (CaM) and calcineurin, a serine/threonine protein phosphatase composed of a catalytic A subunit (CnA) and the calcium binding regulatory B subunit (CnB) (Guerini, 1997). Direct interaction of calcium-bound CaM to its specific binding domain present in the catalytic CnA subunit leads to the activation of the phosphatase calcineurin (Guerini, 1997).

Saccharomyces cerevisiae has served as a model organism to study calcium and magnesium homeostasis and calcium-dependent signaling in fungi. The best-characterized target of calcineurin is the transcription factor (TF) Crz1p. In response to stress, the Ca^{2+}/ calmodulin/calcineurin pathway is activated and leads to the dephosphorylation of Crz1p and therefore its translocation to the nucleus to modulate gene expression. The nucleocytoplasmic trafficking of Crz1p depends on the phosphorylation state of its Nuclear Localization Signal (NLS) and Nuclear Export Signal (NES) (reviewed in (Cyert, 2003)). Previous work from our

laboratory showed that CrzA, the orthologue of Crz1p in filamentous fungi *A. nidulans,* undergoes a similar activation process in response to elevated calcium levels, but also to other divalent cations such as manganese and alkaline pH (Hernández-Ortiz and Espeso, 2013). Furthermore, we demonstrated that the phospho-protein CrzA has different phosphorylation states in response to elevated calcium levels or alkaline pH (Hernández-Ortiz and Espeso, 2013).

In *A. nidulans*, CrzA is properly signalized and transported to nuclei at extracellular calcium concentrations below 0.1 mM (Hernández-Ortiz and Espeso, 2017). However, a null *crzA* strain displays sensitivity to extracellular concentrations of calcium over 10 mM. This fact indicates that CrzA function is mainly required to prevent the negative effects of high extracellular concentrations of calcium (Hernández-Ortiz and Espeso, 2017). CrzA is also required for tolerance of concentrations of manganese above 5 mM and pH values over 7.5 (Hernández-Ortiz and Espeso, 2013). Under these conditions, the null *cnaA* (catalytic subunit of calcineurin) mutant displays an impaired colonial growth with severe morphological defects and sensitivity (Soriani *et al.*, 2008; Hernández-Ortiz and Espeso, 2013). To understand the mechanisms of calcium signalling in *Aspergillus*, Almeida and collaborators selected for suppressor mutations of *crzAΔ* calcium intolerance (Almeida *et al.*, 2013). Mutations in three genes were identified and it was relevant the finding of a mutation, *cnaB2,* affecting the regulatory subunit of calcineurin. The *cnaB2* suppressor mutation was interpreted as conferring calcium tolerance to *crzAΔ* strains through restoration of calcium homeostasis. These results could indicate that in *A. nidulans* there are calcineurin-dependent and CrzA-independent pathways (Almeida *et al.*, 2013).

Calcium homeostasis in *A. nidulans* is greatly influenced by the activity of the transcription factor SltA. The *sltA* deletion strain display sensitivity to high concentrations of Li^+, Na^+, K^+ and Mg^{2+} cations but not to Ca^{2+}. In fact, an elevated extracellular concentration of Ca^{2+} reduces the sensitivity of null *sltA* strains to cations and alkalinity (Spielvogel *et al.*, 2008). Intracellular

calcium storage is also increased in a null *sltA* background and transcriptional analyses of vacuolar calcium ATPases pointed to an important role of these transporters in calcium homeostasis in *A. nidulans*. To date the role of calcium channel MidA/CchA in calcium tolerance and the interplay of Ca^{2+}/Mg^{2+} cations has not been explored in detail in fungi. In this work, we focus on understanding the mechanisms to control calcium homeostasis by studying the suppression of calcium sensitive phenotype of null *crzA* strain and also revisiting previous findings by Almeida and collaborators (2013).

Results

Elevated extracellular levels of magnesium suppress calcium sensitivity displayed by null crzA *mutant.*

SltA is a zinc-finger transcription factor involved in cation homeostasis and tolerance to ambient alkaline pH. The null *sltA* strain is sensitive to elevated levels of extracellular magnesium but no phenotype has been observed under excess of calcium compared to a wild type strain (Mellado *et al.*, 2016). An opposite phenotype was described for the null *crzA* strain (Hernández-Ortiz and Espeso, 2013). However, we detected a cross effect between calcium and magnesium during characterization of both null *sltA* and *crzA* strains.

When medium was supplemented with 200 mM Mg^{2+} the null *crzA* mutant exhibited colonial growth and asexual development (sporulation capacity) comparable to the wild-type strain (Fig. 1A). A mixture of 200 mM Mg^{2+} and 100 mM Ca^{2+} was tolerated by the null *crzA* mutant. Thus, magnesium prevented the negative effect of this large excess of extracellular calcium concentration (Fig. 1A). A similar cross effect was observed with the null *sltA* strain. A concentration of 200 mM Mg^{2+} prevented growth of null *sltA* mutant, but addition of 100 mM Ca^{2+} restored normal colonial growth (Fig. 1A).

To investigate the importance of Mg^{2+} for *sltA* and crzA mutants, we studied the effect of restricting the availability of this cation in the medium. Figure 1B shows that depletion of Mg^{2+} in AMM strongly reduced colonial growth for the three strains analyzed. In fact, the null *crzA* strain displayed a colony morphology that resembled that observed under high calcium concentrations: poor radial growth and accumulation of an orange/brown pigment (compare growth of *crzAΔ* mutant with extra Ca^{2+} in Fig. 1A). This phenotype agrees with observations from other groups that low extracellular levels of Mg^{2+} may cause alterations in cation homoeostasis, by upregulating ENA1, that encodes the P-type ATPase sodium pump, and

PHO89, encoding a sodium/phosphate cotransporter, which are also upregulated under calcium and alkaline stress. It has been proposed that Mg^{2+} starvation causes an increase in cytoplasmic free calcium leading to calcium signaling (Mendizabal *et al.*, 2001; Hu *et al.*, 2007; Wiesenberger *et al.*, 2007). Supplementation with at least 0.2 mM Mg^{2+} was necessary for reconstitution of colony growth of both null *sltA* and *crzA* strains to a similar extent to that observed for the wild-type strain. Thus, these results corroborate that magnesium is an important cation in *A. nidulans* physiology and a cross talk between calcium and magnesium homeostatic pathways may occur.

Absence of functional MidA/CchA calcium channel reduces but not fully suppress calcium sensitivity of null crzA *mutant.*

Calcium tolerance of *crzA⊿* strain depends on the extracellular concentration of this cation (Hernández-Ortiz and Espeso, 2017). As shown on Figure 2, on standard *Aspergillus* minimal medium a colony of null *crzA* mutant displays normal radial growth although poor conidiation compared to the wild type. A continuous reduction in radial growth of null *crzA* mutant was observed when increasing the concentration of extracellular calcium up to 10 mM (less than 20% of radial growth). Above 50 mM Ca^{2+}, growth of *crzA⊿* mutant was completely inhibited (Fig. 2).

A possible explanation for the calcium-sensitive phenotype of *crzA*Δ mutant is that calcium entry through the high affinity calcium channel is not properly regulated. To test this possibility, the effect of deleting calcium channel CchA and its regulatory subunit MidA in a *crzA*Δ background was analyzed. We constructed single and double null *midA*Δ *cchA*Δ mutants and we analyzed them under the same conditions. These *midA*Δ/*cchA*Δ mutant strains did not displayed any sensitivity to high calcium concentrations (Fig. 2). In contrast, on standard AMM

a strong compact colony morphology and poor asexual development was observed. This phenotype is consistent with a lower influx of calcium and limitation of intracellular calcium as observed before (Fig. 1B). Single nulls of both calcium channel subunits in combination with *crzA*Δ were generated. Both *cchA*Δ *crzA*Δ and *midA*Δ *crzA*Δ double mutants grew comparable to WT at calcium concentrations in which the single null *crzA* mutant displayed some degree of sensitivity to this cation (7.5 and 10 mM). In fact, a calcium concentration of 50 mM was now required to observe a similar growth inhibitory effect to that shown by the single *crzA*Δ strain at 25 mM. Thus, loss-of-function of any of both subunits of the calcium channel reduced 2 to 3 times the sensitivity of null *crzA* to calcium (Fig. 2).

The suppressor effect of magnesium was also visible in the absence of a functional calcium channel (Fig. 2). Presence of 100 mM Mg^{2+} suppressed the calcium-sensitive phenotype displayed by strains carrying the *crzA*Δ allele when 50 mM calcium was added. A negative effect of magnesium was not observed in *midA*Δ/*cchA*Δ strains even when medium was supplemented with 200 mM Mg^{2+}, suggesting that magnesium does not obstruct or compete with other remaining calcium uptake mechanisms. These results strongly support the idea that a reduction in calcium uptake together with an increase in intracellular levels of Mg^{2+} may act in concert to prevent the deleterious effect of lacking CrzA activity at high extracellular concentrations of calcium.

Magnesium impinges on the calcium-dependent signaling of CrzA.

CrzA is detected at different phosphorylation levels in SDS-polyacrylamide electrophoresis. CrzA forms with a high level of phosphorylation migrate at a low rate compared to those forms that are dephosphorylated, indicated with $CrzA^{+P}$ and $CrzA^{-P}$ respectively in Fig. 3 (Hernández-Ortiz and Espeso, 2013). Figure 3 displays those changes in

189 the electrophoretic mobility of CrzA-GFP fusion in response to calcium (compare RC, resting
190 cells, and calcium-induced cells). An increase in mobility is observed after 1 min of calcium
191 addition ($CrzA^{-P}$ in Fig. 3) and no qualitative difference was detected between 1 mM or 100
192 mM calcium, showing that 1 mM Ca^{2+} suffices for calcineurin (CN) mediated dephosphorylation
193 of CrzA (Fig. 3). However, recovery of highly phosphorylated states of CrzA ($CrzA^{+P}$) changed
194 with the amount of added calcium. Full recovery of low electrophoretic migration was
195 observed after 30 min upon 1 mM calcium addition. In contrast, after 30 min of exposure to a
196 100-fold concentration of calcium, we detected intermediate states of phosphorylated CrzA
197 (asterisk, Fig. 3A). Figure 3A (bottom) shows an experiment to confirm that the observed
198 electrophoretic changes of CrzA were due to its dephosphorylation. We performed control *in*
199 *vitro* dephosphorylation assays of the low mobility CrzA (RC) by inhibiting the calcineurin
200 activity with the use of cyclosporine A (CsA) (as previously demonstrated in detail, (Hernández-
201 Ortiz and Espeso, 2013). These results indicate that higher levels of intracellular calcium drive
202 to a prolonged active state of CN.
203 In contrast to the effect of Ca^{2+} in reducing CrzA mobility, addition of 100 mM Mg^{2+} had the
204 opposite effect (Fig. 3B). Compared to mobility of CrzA in resting cells, a visible reduction in
205 mobility was observed from 1 min after magnesium addition, indicating that any
206 dephosphorylating mechanism acting on CrzA was attenuated. Next, we analyzed if such Mg^{2+}-
207 dependent attenuation could affect calcium signaling. Cells expressing CrzA-GFP were treated
208 for 30 min with 100 mM Mg^{2+} (RC30), and then either 1 mM or 100 mM Ca^{2+} was added (Fig.
209 3C). Mycelial samples were taken different times and analyzed for the phosphorylation pattern
210 of CrzA. In contrast to the strong dephosphorylating effect when 1 mM Ca^{2+} was added to
211 resting cells, magnesium pre-treated cells showed partial change in CrzA mobility. A stronger
212 effect on CrzA mobility in Mg^{2+} pre-treated cells was observed after addition of 100 mM Ca^{2+}.
213 At 1 min, the high mobility band corresponding to a dephosphorylated form of CrzA was
214 clearly visible, however a low mobility band, corresponding to phosphorylated forms, was

observed in all samples. In fact, the high mobility band reduced its signal over the time. These results show a negative effect of magnesium in calcium signaling over CrzA by preventing its Ca^{2+}-induced dephosphorylation. Taking the post-translational modification process of CrzA as a model, these results suggest that Mg^{2+} has a regulating role in the activity of calcineurin, opposing the activating effect of calcium.

Magnesium modifies the nuclear import dynamics of CrzA.

The graph shown in Figure 4A illustrates the effect of adding either 1 mM or 100 mM calcium in the nuclear accumulation of the functional fluorescent CrzA fusion. Nuclear fluorescence was measured and compared to cytoplasmic fluorescence at different times along 30 minutes after addition of the cation. In contrast to calcium, a large concentration of magnesium does not induce nuclear entry of CrzA (white bars, Fig. 4A) while 1 mM or 100 mM produced a comparable effect on promoting nuclear accumulation of CrzA (light and dark grey bars, respectively, Fig. 4A), as was noticed before (Hernández-Ortiz and Espeso, 2013; Hernández-Ortiz and Espeso, 2017). In the previous section, we show that calcium-dependent signaling of CrzA is blocked in the presence of magnesium. Predictably, accumulation of highly phosphorylated forms would result in the exclusion of CrzA from nuclei since dephosphorylation is required for its nuclear transport (Hernández-Ortiz and Espeso, 2013; Hernández-Ortiz and Espeso, 2017). Quantitative measurements of nuclear vs cytoplasmic fluorescence of a strain expressing CrzA-GFP demonstrate that magnesium largely prevents nuclear entry of CrzA when 1 mM calcium is added (stripped bars, Fig. 4B). This magnesium-dependent effect is also dependent of calcium concentration. A 100 times higher concentration of Ca^{2+} still has the capacity to promote nuclear accumulation of this transcription factor (dotted bars, Fig. 4B), although delayed and transient. In agreement with

previous immunodetection data, magnesium attenuates the calcium-induced dephosphorylation of CrzA and consequently the timely activation of nuclear transport signals.

Role of calcineurin in the calcium-hypersensitivity phenotype caused by null crzA *allele. Inhibiting the activity of CN.*

Due to the negative effect of Mg^{2+} on the calcium-dependent signaling of CrzA, we analyzed whether attenuation of CN activity could suppress calcium sensitive phenotype of *crzA*Δ strain. Using a concentration of 10 μM cyclosporine A (CsA), a well-known inhibitor of CN, we observed a strong reduction of colony diameter of a wild-type strain, and a similar inhibitory effect was observed for a *crzA⊿* mutant, *sltA⊿* and double *cchA⊿ crzA⊿* and *midA⊿ crzA⊿* mutants (Fig. 5A). This CsA effect on colony morphology was similar to the phenotype observed before for a strain lacking of the calcineurin subunit CnaA (Hernández-Ortiz and Espeso, 2013). All null *crzA* strains used in this experiment showed the expected sensitivity to 100 mM calcium, however, addition of CsA improved colonial growth to a similar extend to that observed for the wild type, although largely differs to the positive effect of adding magnesium (see controls marked by the red box, Fig. 5A). Fig. 5B shows a quantitative experiment of the effect on mycelial growth caused by calcium in the previous mutant backgrounds, confirming colonial growth tests. Calcium caused a strong reduction in mycelial mass in the absence of CrzA activity. As for colonial growth, inhibition of calcineurin by CsA relieves the negative effect of calcium increasing mycelial masses for the three null *crzA* strains tested. We conclude that attenuation of calcium sensitivity of null *crzA* by addition of cyclosporine A suggests that calcineurin activity must be a deregulated element in the *crzA⊿* mutant background under high calcium concentrations.

Role of calcineurin in the calcium-hypersensitivity phenotype caused by null crzA *allele; reviewing the phenotype of* cnaB2 *mutation.*

A mutation in the calcineurin regulatory subunit, *cnaB2*, was isolated as a suppressor of calcium sensitivity of null *crzA* mutant (Almeida *et al.*, 2013). To study the effect of *cnaB2* mutation in the signaling of CrzA in a loss-of-function *crzA* background, we took advantage of the GFP-CrzA(1-448) chimera. This truncated form lacks the DNA binding domain and the mutant expressing this truncated version of CrzA displays a null *crzA* phenotype (Fig. 6A). However, GFP-CrzA(1-448) is a target of CN becoming dephosphorylated when calcium is added and subsequently displays nuclear accumulation (see (Hernández-Ortiz and Espeso, 2013)). In addition, this truncated GFP-tagged version of CrzA is expressed ectopically and consequently we can study its signaling in the presence or absence of the endogenous CrzA protein. Figure 6A shows the differential sensitivity to calcium of MAD2168 strain expressing GFP-CrzA(1-448) chimera in a *crzA*+ background and of MAD2172 that carries a null *crzA* allele. The presence of a endogenous copy of *crzA* suppresses the sensitivity to calcium displayed by the only expression of GFP-CrzA(1-448). The calcium-sensitive phenotype of MAD2172 (*crzA*(1-448) *crzA⊿*) can also be suppressed by the *cnaB2* mutation. A *cnaB2 crzA*(1-448) *crzA⊿* mutant (MAD5514) is able to grow on media containing 50 mM Ca^{2+} as it is the double *cnaB2 crzA⊿* strain (MAD5537/rev2) (Fig. 6A). These phenotypic analyses showed that *cnaB2* suppresses the calcium sensitive phenotype independently of presence of ectopically expressed CrzA(1-448).

Diverse forms of the GFP-CrzA(1-448) chimera are immunodetected in protein extracts of resting cells of strain MAD2172 (*crzA⊿*) indicating that CrzA(1-448) was found in different states of phosphorylation (Fig. 6B lane 3). Addition of 50 μM CsA largely reduced the mobility of GFP-CrzA(1-448) chimera to a single band, evidencing that CN activity participates on the phospho-turnover of this fusion protein (Fig. 6B, compare lanes 3 and 4). Addition of Mg^{2+} also

293 altered the mobility of CrzA(1-448) and a well-defined slower mobility band was detected
294 when increasing concentrations of Mg^{2+} were added (Fig. 6B lanes 1-4). Presence of *cnaB2*
295 mutation causes a reduction in the mobility of CrzA(1-448) comparable to the effect of adding
296 CsA (Fig. 6B, compare lanes 4 and 5). Addition of 1 mM or 100 mM calcium has no effect on
297 the *cnaB2* mutant and the mobility of CrzA(1-448) remained unaltered (Fig. 6B, lanes 5-9). A
298 dephosphorylation experiment using lambda protein phosphatase (λPP, Fig. 6C) showed the
299 presence of phosphorylated forms of CrzA(1-448) in resting cells of *cnaB2* strain MAD5515 but
300 not in extracts from strain MAD2172. These results demonstrate that *cnaB2* constitutes a loss
301 of CN function and that a proper signaling of CrzA is abolished in this mutant background. The
302 electrophoretic mobility of CrzA(1-448) also changes when a functional form of CrzA is present
303 in the cell. Mobility of CrzA(1-448) in resting cells of strain MAD2168 is comparable to that
304 found in MAD2172 in the presence of CN inhibitor CsA (Fig. 6B, compare lanes 10 and 4). The
305 dephosphorylation experiment shown in Fig. 6C demonstrate the presence of phosphorylated
306 forms of CrzA(1-448) in the presence of a wild-type CrzA protein (strain MAD2168).
307 Magnesium has a minor effect on the mobility of CrzA (1-448) in the presence of functional
308 CrzA (lanes 10, 12 and 13, Fig. 6B). Instead, addition of CsA increased the reduced mobility of
309 CrzA(1-448) in a *crzA*$^{+}$ background. These results indicate that phosphorylation levels of
310 CrzA(1-448) also depend on the CrzA activity, finding lower phosphorylation levels in the
311 absence of CrzA. In addition, the observed effect of CsA on the mobility of CrzA(1-448) in the
312 presence or absence of CrzA strongly supports the idea that calcineurin activity is increased in
313 a cell that lacks of a functional form of CrzA.
314
315 *Phosphoproteomic studies of functional and non functional versions of CrzA*
316
317 The possibility that truncated forms of CrzA might be modified by calcineurin depending on
318 their functional grade determined that we analyzed phosphorylated residues in two truncated

319 forms, the non-functional form CrzA(1-448) and the functional form CrzA(1-612). A global
320 phosphoproteomic analysis (to be published elsewhere) revealed several phosphopeptides for
321 the functional form of CrzA, while none were observed in the non-functional form (Fig. 7A;
322 Table S1). To validate these results we compared the presence in our samples of
323 phosphopeptides of other proteins predictably regulated by phosphorylation such as the
324 plasma ATPase PmaA and the ammonium transporter MepA (Estrada *et al.*, 1996; Reoyo *et al.*,
325 1998; Monahan *et al.*, 2002; Boeckstaens *et al.*, 2014) (Supporting material, Table S1). At least
326 eleven serine residues were differentially found to be phosphorylated in the form CrzA(1-612)
327 (Fig. 7A). These serine residues were identified into four peptides from a region between
328 coordinates 379 and 467, upstream of the DNA binding domain (Fig. 7B). This region was
329 already predicted to be highly phosphorylated and contains the functional site for calcineurin
330 docking, CDD2 (Hernández-Ortiz and Espeso, 2013) (Fig. 7B). In the absence of calcineurin
331 activity, we detected at least seven potential phosphorylated serine residues in the form
332 CrzA(1-612), most of them in common with those identified in the presence of a functional
333 calcineurin (Fig. 7).
334 As determined before, the presence of *cnaB2* elevated the phosphorylation levels of CrzA(1-
335 448). The phospho-proteomic analysis of protein extract from resting cells of CrzA(1-448)
336 *cnaB2* mutant (MAD5514) confirmed that result. We detected phosphorylated serine residues
337 in two peptides close to CDD2 also found to be modified in CrzA(1-612). The overall
338 phosphoproteomic data confirms that CrzA is phosphorylated at various serine residues
339 located in the proximity to the functional calcineurin domain in CrzA and that a non-functional
340 CrzA is mainly in a dephosphorylated state.
341
342
343 *Lack of effect of calcium, magnesium and alkaline pH on the CnaB electrophoretic mobility and*
344 *cellular localization.*

CnaA has been shown to accumulate in septa and cytoplasmic aggregates (Hernández-Ortiz and Espeso, 2017). We tagged CnaB with GFP epitope to follow its localization and electrophoretic mobility in response to the calcium, magnesium and alkalinity. Recombinant strains expressing CnaB-GFP showed a wild-type phenotype. Immunodetection experiments showed a single band of a size of 52 kDa for the tagged CnaB-GFP protein, in both wild type (MAD5502, Fig. S1A) and null *crzA* background (MAD5507, data not shown). Mobility of CnaB-GFP remained unchanged when medium was alkalinized or supplemented with magnesium or calcium (Supporting material, Fig. S1A).

Microscopy analysis of cells expressing CnaB-GFP showed that the regulatory subunit had the same localization as the catalytic module, accumulating at both sides for septa and in cytoplasmic aggregates ((Hernández-Ortiz and Espeso, 2017), Supporting material, Fig. S1B). These localizations remained unaltered when cations were added or pH was alkalinized (not shown). The results indicate that, if modulation of CN activity occurs upon stress, this is independent of its cellular localization.

Transcriptional control of the regulator of calcineurin activity, rcnA*.*

A key element in regulating the activity of CN is the highly conserved RCN factor, also known as calcipressin (Görlach *et al.*, 2000). In *S. cerevisiae*, expression of RCN1 is positively regulated by Crz1p (Kingsbury and Cunningham, 2000; Mehta *et al.*, 2009). A homologue in *A. nidulans* has been described, *rcnA*, but its regulation by CrzA has not been determined (Almeida *et al.*, 2013). We have analyzed the expression levels of *rcnA* in a wild type background (Fig. 8). Transcription of *rcnA* is detected in mycelium grown in standard minimal medium. Depletion of Mg^{2+} caused a small reduction in *rcnA* levels (ratio *rcnA* vs 18S rRNA, 18.5 and 11.8,

371 respectively). In contrast, 10 min after addition of 10 mM Ca^{2+} greatly increased expression of
372 *rcnA* (41.6 vs 18.5). This increase in expression could be due to calcium-induced
373 dephosphorylation and activation of CrzA nuclear import. Thus, presence of Mg^{2+}, that
374 prevents dephosphorylation and nuclear import of CrzA, should reduce expression of *rcnA*.
375 Northern analysis shows that this is the case and addition of 200 mM Mg^{2+} alone or together
376 with calcium largely reduced expression levels of *rcnA* (3.1 and 8.4, respectively) compared to
377 the levels found in control medium (18.5) or in the presence of calcium (41.5). These results
378 support a regulation of *rcnA* expression dependent on CrzA activity. Then, we analyzed
379 expression levels of *rcnA* in a null *crzA* background. Northern analysis showed that expression
380 of *rcnA* was downregulated in the absence of CrzA function. Expression levels of *rcnA* in
381 standard minimal medium reduced in the null *crzA* strain compared to WT (5.9 vs 18.5).
382 Calcium did not increased expression of *rcnA* and either depletion or addition of 200 mM of
383 Mg^{2+} did not affect expression of *rcnA*. The overall data indicates that CrzA is responsible of
384 *rcnA* regulation although expression is continuously detected. Thus, RcnA must be present at
385 basal level in the cell irrespective of CrzA activity, however, calcium induces expression and it
386 is expected an elevation of RcnA protein levels, supposedly involved in controlling activity of
387 CN after its induction by calcium.
388
389
390 **Discussion**
391
392 Calcium is a key messenger and the signaling pathway is well conserved along phylogeny. In
393 fungi, an effector of calcium signaling is the family of transcription factors Crz, which are
394 substrates of calcineurin phosphatase. In *A. nidulans*, *crzA* mutants tolerate a limited amount
395 of extracellular calcium (Hernández-Ortiz and Espeso, 2013) and similar calcium
396 hypersensitivity is observed for other Crz homologues from *S. cerevisiae*, *C. albicans*, *S. pombe*

397 and *A. fumigatus* (Hirayama *et al.*, 2003; Zakrzewska *et al.*, 2005; Karababa *et al.*, 2006; Soriani
398 *et al.*, 2008). However, it has been intriguing the partial tolerance of a *crzA* mutant to
399 moderate (10 mM) concentrations of calcium, indicating a need of CrzA activity mainly under
400 large excess of extracellular calcium, thus we have focused on elucidating the basis of this
401 partial tolerance to calcium.
402 A predicted role of CrzA is to prevent an excessive cytoplasmic accumulation of calcium as a
403 result of massive entry through calcium uptake systems (Almeida *et al.*, 2013). The accepted
404 model of calcium homeostasis for most organisms contemplates that the inadequate
405 cytoplasmic accumulation of calcium constitutes a source for deregulation of important
406 cellular processes and thus affecting cell viability (Cui and Kaandorp, 2006; Cui, Kaandorp,
407 Sloot, *et al.*, 2009; Tisi *et al.*, 2016). As in yeast, the principal system for entry of calcium into *A.*
408 *nidulans* cells is the putative voltage-gated Ca^{2+} channel (VGCC) composed of the CchA and
409 MidA proteins (Wang *et al.*, 2012). Wang S and collaborators found that these channels play
410 important roles in conidiation, hyphal polarity and cell wall components in *A. nidulans* (Wang
411 *et al.*, 2012). They demonstrated that depletion of CchA /MidA resulted in conidiation defects
412 in an inoculum-size-dependent way and interestingly these conidiation defects can be rescued
413 by extracellular Ca^{2+} in a calcineurin-dependent way. This observation is also confirmed from
414 our growth plates assays (Fig. 2). Here we show that a reduction of calcium uptake by lacking
415 the VGCC activity ameliorates the sensitive phenotype displayed by the null *crzA* and
416 reinforces the idea that excessive availability of free cytoplasmic calcium could be a cause for
417 this sensitivity.
418 In *A. nidulans* we have identified another transcription factor involved in calcium homeostasis,
419 SltA (Spielvogel *et al.*, 2008). Opposite to the phenotype displayed by *crzA⊿* mutant, null *sltA*
420 strains tolerate elevated extracellular concentrations of calcium due, most probably, to the
421 high capacity of *sltA* mutant to store this cation at intracellular compartments (Findon *et al.*,
422 2010). When studying tolerance to other divalent cations, we observed that magnesium

causes an opposite effect in null *crzA* and *sltA* strains. Excess of extracellular magnesium contributes to a better colonial growth of null *crzA* strain also improving asexual development, while inhibits colonial growth of a null *sltA* mutant (Spielvogel *et al.*, 2008). Interestingly, a mixture of both divalent cations mitigate respective sensitive phenotypes for both null mutant strains suggesting an overlap of homeostatic or regulatory mechanisms for both cations. Here we focused in those related to CrzA TF. The cross interaction between Mg^{2+} and Ca^{2+} that we describe in *A. nidulans* was also found in *S. cerevisiae*. Cui and collaborators (2009) described that sensitivity displayed by a *pmc1* mutant to high calcium concentrations was dependent on the medium composition, and particularly to the presence of magnesium cation (Cui, Kaandorp, Ositelu, *et al.*, 2009). These authors found that alternative calcium transport systems are also under the regulation of magnesium. In our study, we found a positive effect of magnesium in tolerance to calcium and enhancing *A. nidulans* growth even in the absence of a functional VGCC system, thus magnesium has no particular negative effect in this fungus when the Slt regulatory system is functional.

At other level of possible crosstalk between magnesium and calcium are signaling proteins in the calcineurin (CN) activation system. CN activity is affected by a deregulated level of cytoplasmic calcium. Our work measures activity of CN by detecting the diverse posttranslational forms of CrzA (Hernández-Ortiz and Espeso, 2013). Absence of CN activity renders a highly phosphorylated version of CrzA that has a particularly low electrophoretic mobility. Sudden elevation of extracellular calcium rapidly activates CN and one derived effect is the increase in electrophoretic mobility of CrzA and its nuclear accumulation. Dephosphorylated forms of CrzA display a markedly higher mobility (this work and (Hernández-Ortiz and Espeso, 2013)). Importantly, as shown before, signaling of CrzA occurs within a wide range of calcium concentrations, some of which are well below the sensitive concentration of 10 mM (see this work and (Hernández-Ortiz and Espeso, 2017)) however, calcium concentration seems to govern only the duration of this signaling. We demonstrate

449 that Mg^{2+} prevents dephosphorylation of CrzA and has this effect also when calcium is added.
450 Indicating that Mg^{2+} might well contribute to CN inactivation. Thus, we focused on the
451 hypothesis that loss of CrzA function generates deregulated state of CN. We revisited the
452 phenotype exhibited by the *cnaB2* mutant. A mutation in the regulatory subunit of CN was
453 isolated as a suppressor of the calcium sensitive phenotype. Initially, this phenotype was
454 explained as the *cnaB2* suppressor mutation confers calcium tolerance to *crzAΔ* strains
455 through restoration of calcium homeostasis (Almeida *et al.*, 2013). Here we show that
456 phosphorylated levels or CrzA are elevated in the *cnaB2* mutant background. Thus, CN is
457 downregulated in a *cnaB2* mutation. Phosphoproteomic studies have revealed multiple serine
458 residues potentially modified in CrzA from resting cells (Fig. 7), as it was previously expected
459 (Hernández-Ortiz and Espeso, 2013). Importantly, the presence of a functional CrzA protein is
460 key to maintain those serine residues in such modified state. These studies also support our
461 conclusion that *cnaB2* reduces CN activity (Fig. 7, Table S1). This mutation points to the excess
462 of CN as an important cause of the calcium sensitive phenotype. CnaB2 acts at the level of
463 posttranslational modifications occurring at CrzA but cannot be excluded that a mutant CnaB2
464 form might modify CN activity in a way to interfere with calcium homeostasis in a CrzA-
465 independent basis. Future experimentation on the effects of *cnaB2* mutation may explore
466 these possibilities and additional targets of CN.
467 How Mg^{2+} suppresses calcium sensitive phenotype? Which are the possible roles of
468 intracellular Mg^{2+}? Our results fit well with the regulatory role of Mg^{2+} described in *S.*
469 *cerevisiae* (see revision by (Cyert and Philpott, 2013; Espeso, 2016)). In yeast, Mg^{2+} act at three
470 levels, reducing the intracellular pool of Ca^{2+} and the release from the internal stores, and the
471 competition with Ca^{2+} to the EF-hands present in regulatory proteins such as calmodulin and
472 calcineurin regulatory subunit (Grabarek, 2011). There are several biochemical and biophysical
473 works identifying magnesium-binding sites to calmodulin and its role on target recognition by
474 calmodulin. Ohki et al., found that magnesium preferentially binds to calcium binding sites I

475 and IV of calmodulin in the absence of calcium and that calcium binding site III displays the
476 lowest affinity for magnesium (Ohki *et al.*, 1997). In contrast to the marked structural
477 transitions induced by calcium binding, magnesium-binding causes only localized
478 conformational changes within the four calcium-binding loops of calmodulin, not able to cause
479 interaction of CaM with target proteins. They also found that the binding of calcium-saturated
480 calmodulin to target peptides is affected by magnesium with the binding affinity decreasing as
481 the magnesium concentration increases. We propose in *A. nidulans* a similar regulatory role
482 for Mg^{2+} by modulating the activity of the regulatory subunit of CN through competition with
483 Ca^{2+} at the EF hands. The phenotype displayed by *cnaB2* mutation shows the importance of a
484 correct folding of EF-hand-II in the activity of CnaB. Substitution of Ca^{2+} at EF-hand II by Mg^{2+}
485 could be a key process to modulate CN activity.
486 Is calcipressin RcnA a missing factor in a null *crzA* background? Two RCN proteins are found in
487 *S. cerevisae* and had diverse roles in regulating CN activity. RCN1 may act as both negative and
488 positive modulator of CN and RCN2 is a negative one. Crz1p was demonstrated to modulate
489 the transcription of these calcineurin regulators (Kingsbury and Cunningham, 2000; Mehta *et*
490 *al.*, 2009). In *A. nidulans* and *A. fumigatus* a single gene (*rcnA*) coding for a member of this
491 family of negative calcineurin regulators was described (Soriani *et al.*, 2008). We studied the
492 expression levels of *rcnA* in a wild-type and null *crzA* background. Expression of *rcnA* is
493 detected in both genetic backgrounds indicating the presence of a basal level of RcnA in the
494 absence of CrzA function. This is important because those low/basal levels of calcipressin could
495 be modulating CN activity at low calcium concentrations. However, an elevation of RcnA levels
496 seem to be required when calcium is present. Northern analyses show that *rcnA* expression
497 greatly elevates when calcium was added, and that this change in expression pattern was
498 dependent on CrzA. Upregulation or *rcnA* is interesting because the "active" form of
499 calcipressin has a lower lifetime (Genesca *et al.*, 2003) and turnover of RcnA must be
500 accelerated to maintain appropriate levels of CN activity. However, this negative feedback is

broken in a null *crzA* mutant. Upregulation of RcnA is lost in the null *crzA* mutant, supporting the conclusion that mechanisms of control of CN activity are missing in *crzA* mutant background.

Figure 9 depicts an integrative model of our findings on how to turn CN activity off in *A. nidulans*. CrzA plays an important role by regulating the expression of *rcnA*. In agreement with its proposed role as a negative regulator or CN activity in *A. nidulans* (Soriani *et al.*, 2008), expression of *rcnA* is elevated in the presence of calcium. In this model of regulation, RcnA levels in the cell must be increased as an immediate response to the induction of the CN-CrzA system. CrzA plays an important role here and modulates the production of the regulator of CN activity in addition to calcium homeostasis, most probably through expression of calcium transporters. Magnesium plays also a key role in the system by releasing Ca^{2+} from the holo-version of CnaB and probably CaM, conducting to an inactive form of CN. Absence of CrzA causes a major distortion of these regulatory circuits and, in the presence of calcium, the hyperactivation of CN and subsequent failure to conduct the adequate regulation or other pathways dependent on CN activity.

Conclusions

In this work, we proved that a mixture of calcium and magnesium mitigate respective sensitive phenotypes in null *crzA* and *sltA* mutant strains, due to possible overlapping homeostatic or regulatory mechanisms for both cations. We further confirmed our hypothesis that loss of CrzA function generates deregulated state of CN. By using a *cnaB2* suppressor mutation, which confers calcium tolerance to *crzAΔ* strains, we showed that phosphorylated levels of CrzA are elevated in this mutant background. Furthermore, taken in account the lost upregulation of

RcnA in the null *crzA* mutant, we propose that excess of calcineurin could be the main cause of the observed calcium sensitive phenotype.

Experimental Procedures.

Strains and media

The *Aspergillus nidulans* and *Escherichia coli* strains used in this work are listed in Table 1 and for the gene nomenclature, we based at (Clutterbuck, 1993). *A. nidulans* strains were grown routinely in appropriately supplemented standard minimal medium (AMM) and complete medium (ACM) at 37°C as described by Cove (Cove, 1966). The solid ACM medium was mainly used for propagation/obtaining conidiospores and maintenance of the strains. Solid AMM properly supplemented was used to characterize the phenotypes of the different mutations of interest (for more details see the section of growth assays on plate). In all experiments in this work calcium and magnesium supplementation was done by adding the respective chloride salts, usually from concentrated stock solutions sterilized by filtration. Sensitivity to calcium and magnesium salts or alkaline pH were scored after culturing the strains for two days at 37°C and then photographed. Colony growth of mutant strains was compared with that of the parental and wild type strains.

Generation of recombinant strains

Standard molecular biology techniques were performed (Sambrook *et al.*, 1989). The oligonucleotides used in this work are listed in Table 2. The *A. nidulans* recombinant strains were obtained by transformation following the protocol described in (Tilburn *et al.*, 1983) or by crossing. For deletion or tagging we used the targeted direct gene replacement technique using the protocol described in (Nayak *et al.*, 2006; Markina-Iñarrairaegui *et al.*, 2011). Essentially, linear DNA cassettes were generated by fusion PCR. Fragments of 1.5 kb

553 comprising the 5'UTR and 3'UTR of a target gene were amplified by using specific primers
554 following the strategies shown in Fig. S2. The fragments for the homologous recombination,
555 were fused to a prototrophic selectable marker (SM, *Aspergillus fumigatus pyrG* or *riboB* loci,
556 indicated as *pyrG*^{Af} and *riboB*^{Af}, respectively) (Markina-Iñarrairaegui *et al.*, 2011). Gene
557 replacements were favored by the presence of null *nkuA* allele (Nayak *et al.*, 2006). Pyrimidine
558 or riboflavin prototrophs were selected and homokaryotic transformants carrying single-copy
559 integration events were identified by PCR, Southern blotting or sequencing procedures. Strain
560 MAD1427 was used as recipient for transformation of *midAΔ*::*riboB*^{Af} or *cchAΔ*::*riboB*^{Af}
561 cassettes to generate strains MAD2740 and MAD2741, respectively. To generate the double
562 null *midA cchA* mutant, two cassettes were cotransformed in MAD1427 resulting in a
563 *midAΔ*::*riboB*^{Af} and *cchAΔ::pyrG*^{Af} alleles (strain MAD2742). To construct double null mutant
564 involving *crzA* and each subunit of the calcium channel, *cchA* and *midA*, we transformed strains
565 MAD2740 and MAD2741 with a DNA cassette containing the 5'UTR of *crzA* fused to the *pyrG*^{Af}
566 gene and to the 3'UTR region of *crzA*. This DNA cassette was obtained by using PCR and
567 oligonucleotides CrzA(1) and CrzA(4) (Hernández-Ortiz and Espeso, 2013) and genomic DNA
568 from strain MAD2842. After transformation, strains MAD2843 and MAD2844 were selected as
569 double *crzA midA* and *crzA cchA* null mutants, respectively.
570 As previously described (Nayak *et al.*, 2006) and Fig. S2B, for CnaB tagged strains, we
571 transformed MAD1425 strain (wild-type *crzA* strain) and MAD3709 (*crzA*Δ strain), with the
572 CnaB-GFP cassette by using *pyrG*^{Af} as a selection marker and we obtained the MAD5501 and
573 MAD5507 strains, respectively. Following the strategy for epitope tagging, Fig. S2B, we
574 obtained a strain expressing the mutant CnaB2 protein fused to HA/*pyrG*^{Af} (MAD5514) by using
575 as recipient MAD5513 strain. MAD5513 was selected among progeny of a crossing event
576 between the strains MAD3709 and MAD2172, and was properly verified by PCR and Southern
577 blotting before use.
578

579 *Protein extraction and analysis procedure*

580 For total protein extractions, strains were cultivated in appropriately supplemented
581 fermentation media for 16 h at 37°C under agitation. Then, different stimulus were added to
582 the culture medium as figured from 1 to 100 mM Ca^{2+}, 100 to 200 mM Mg^{2+}, 50 μM calcineurin
583 inhibitor (CsA) and further incubated from 1 to 30 min, as indicated in the text. In each time
584 point as mentioned, mycelia were collected by vacuum filtered using 0.45 μm pore size
585 nitrocellulose membranes (Scharlau) and frozen in dry ice. Frozen samples were lyophilized for
586 16 h before protein extraction. In order to prevent protein degradation, the alkaline lysis
587 extraction procedure was used as previously tested by (Hernández-Ortiz and Espeso, 2013).
588 For Western blotting proteins were resolved in 4-15% Mini PROTEAN® TGX ™ precast
589 polyacrylamide gels (Biorad) and subsequently transferred to nitrocellulose filters using Trans-
590 Blot®Turbo™ Transfer System (Biorad). Proteins tagged with GFP were detected using a
591 polyclonal mouse anti-GFP (1/5000; clones 7.1 and 13.1; Sigma-Aldrich). Calcineurin regulatory
592 subunit fused to HA was detected using a monoclonal rat anti-HA (1:1000; clone 3F10; Sigma-
593 Aldrich). Peroxidase conjugated goat secondary antibody anti-mouse IgG immunoglubin
594 (1/4000, Jackson Immuno Research Laboratories) or anti-rat IgG +IgGM (1:4000; Southern
595 Biotech) were used to detect primary antibodies. The peroxidase activity was detected with
596 Amersham Biosciences ECL kit and luminescence detected and recorded using a LAS3000
597 imager system (Fuji). The images were analyzed using the Multi-Gauge V3.0 (Fuji) and
598 Coreldraw X7 softwares.

599 For lambda protein phosphatase (λPP) induced dephosphorylation of protein extracts, we used
600 the protocol described in (Hernández-Ortiz and Espeso, 2013).

601

602 Phosphoproteomic procedures

603 For determination of phosphorylated serine and threonine residues the starting material were
604 total protein extracts obtained by the alkaline-lysis protocol described in (Hernández-Ortiz and

605 Espeso, 2013). From each sample, 300 µg of total protein were precipitated with
606 trichloroacetic acid and suspended in 8 M urea, 50 mM ammonium bicarbonate. Proteins were
607 reduced with 10 mM dithiothreitol for 30 min at room temperature (RT), alkylated with 50 mM
608 iodoacetamide in the dark for 30 min at RT, and digested with 15 µg of trypsin overnight at
609 37°C. Peptides mixtures were desalted using C18 SEP-PAK columns. Samples were dried in
610 speed-vac at RT. For phosphopeptide enrichment, TiO_2 affinity chromatography was
611 performed (Boulousis *et al.*, 2011). Briefly, slurry of Titansphere TiO_2 (5 µm) beads was
612 equilibrated in TiO_2 binding buffer; 300 mg/ml lactic acid, 53 % acetonitrile (ACN), 0.07 %
613 trifluoroacetic acid (TFA) at ratio of 25 mg slurry/ml buffer. Peptides were dissolved in 600 µl
614 TiO_2 binding buffer and 72 µl of the Titanium slurry were added to each sample, further
615 incubated during 30 min at RT with end-over-end rotation. Beads were collected by
616 centrifugation and suspended in 150 µl of TiO_2 binding buffer and transferred on top of C8
617 disks Stage Tips, prepared as in (Rappsilber *et al.*, 2007). Using a syringe, beads were drained
618 at 20 µl/min and washed with 150 µl of TiO_2 binding buffer. An additional washing step was
619 carried out using 100 µl of a solution of 80 % ACN, 0.1 % TFA. Bound phosphopeptides were
620 eluted using two steps of 50 µl of 0.5 % NH_4OH, collecting each eluate in 100 µl 2 % TFA.
621 Phosphopeptide-enriched samples were speed-vac dried and reconstituted in 0.1 % TFA for
622 desalting using C 18 Zip-Tip columns.
623 For MS analysis, fractions of 1/6 from each phosphopeptide-enriched sample were analyzed by
624 nano-LC-MS/MS. Peptides were trapped onto a AcclaimPepMap 100 C18 (2 cm) precolumn
625 (Thermo-Scientific), and then eluted onto a AcclaimPepMap 100 C18 column (inner diameter
626 75 µm, 25 cm long, 3 µm particle size) (Thermo-Scientific) and separated using a 180 min
627 gradient (0-21 % Buffer B 60 min; 21 %-35 % Buffer B 100 min, 95 % Buffer B 10 min, and 0 %
628 Buffer B 10 min). (Buffer A: 0.1 % formic acid/2 % ACN; Buffer B: 0.1 % formic acid in ACN) at a
629 flow-rate of 250 nL/min on a nanoEasy HPLC (Proxeon) coupled to a nanoelectrospray ion
630 source (Thermo-Scientific). Mass spectra were acquired on a LTQ-Orbitrap Velos mass

631 spectrometer (Thermo-Scientific) in the positive ion mode. Full-scan MS spectra (m/z 400–
632 1,500) were acquired in the Orbitrap at a resolution of 60,000 at 400 m/z and the 15 most
633 intense ions were selected for collision induced dissociation (CID) fragmentation in the linear
634 ion trap with a normalized collision energy of 35 %. Singly charged ions and unassigned charge
635 states were rejected. Dynamic exclusion was enabled with exclusion duration of 30 s. Mass
636 spectra *.raw files were searched against an Anidulans.fasta database (10,720 protein entries)
637 using Sequest search engine through Proteome Discoverer (version 1.4.0.288, Thermo
638 Scientific). Search parameters included a maximum of two missed cleavages allowed,
639 carbamidomethylation of cysteines as a fixed modification and N-terminal acetylation, C-
640 terminal oxidation and serines, threonines and tyrosines phosphorylation as variable
641 modifications. Precursor and fragment mass tolerance were set to 10 ppm and 0.6 Da,
642 respectively. As scoring algorithm, node 3 phosphoRS was used to evaluate the statistical
643 confidence of location of phosphorylation sites. Identified peptides were validated using
644 Percolator algorithm with a q-value threshold ≤ 0.01 as described in (Käll *et al.*, 2007).
645
646 *Growth assays on solid medium.*
647 We studied the sensitivity of the recombinant *A. nidulans* strains to salt / cations and
648 calcineurin inhibitor. Firstly, the colony growth was studied by point inoculating conidiospores
649 on solid AMM supplemented with the appropriate stress condition as indicated in the figures
650 from 1 - 100 mM Ca^{2+}, 0.02 - 200 mM Mg^{2+} (both as chloride salts as indicated above) and
651 incubated at 37°C for 2 days. In addition, using 24-multiwell plates containing 1 ml of AMM
652 plus the stress of interest; 100 mM Ca^{2+}, 200 mM Mg^{2+} and 10 μM immunosuppressant
653 Cyclosporin A (CsA) were used as an additional tool of sensitivity screening (Sebastián-Pérez *et*
654 *al.*, 2016). CsA (Sigma-Aldrich) stock was prepared in dimethyl sulphoxide. 10^3 spores of
655 *Aspergillus*, calculated using a Neubauer chamber, were centrally inoculated on each well. The
656 plates were incubated at 37°C for 2 days and then photographed.

Gene expression analyses

Wild type (MAD2666) (Garzia *et al.*, 2013) and mutant (MAD2448) strains were cultivated in liquid minimal medium for 16 h at 37°C under agitation (250 rpm). Then, different stimulus was added to the culture medium; 200 mM Mg^{2+}, 10 mM Ca^{2+}, and their combination and further incubated for 10 minutes. Where figured $–Mg^{2+}$, we refer in AMM medium without magnesium, which was properly prepared. Total RNA extraction and Northern blot analyses were carried out following standard protocols (Garzia *et al.*, 2009). Briefly, the mycelia were harvested by filtration using Miracloth (Calbiochem, Merck-Millipore, Darmstadt, Germany) and were rapidly frozen in liquid nitrogen. TRIreagent (Fluka, Sigma-Aldrich) was added and we further processed according to the manufacture´s protocols. We checked the integrity and concentration of the resulted RNA samples using a Nanodrop spectrophotometer and we proceeded to Northern blot assays. *rcnA* transcript was detected by using specific genomic probes (oligonucleotides listed in Table 2). Finally, mRNA-DNA hybridization was detected by using a PhosphorImager FLA-5100 plate Reader (FujiFilm). Furthermore, band quantification intensities were performed by using Multi-Gauge V3.0 software (FujiFilm) (Mellado *et al.*, 2015).

Microscopy

For all microscopy experiments, *A. nidulans* conidia were germinated on uncoated μ-Slide 8 well (Ibidi GmbH, Germany) for a direct observation of cultures which contained appropriately supplemented watch minimal medium (WMM) (Peñalva, 2005) and incubated at 25°C for 16 h. After this period, the medium was replaced with fresh one supplemented with different stimulus when indicated, from 1 to 100 mM Ca^{2+} or/and 200 mM Mg^{2+}. In the case of figure 6, photographs were taken of several cells in the same field at the indicated times. The fluorescence was measured in a specific region of the nucleus and compared with a region of

similar area in the nearest cytoplasm. At least 10 cell compartments were imaged and nuclear and cytoplasmic fluorescence were compared in three nuclei of each cell. A Leica DMI-6000b inverted microscope equipped with Normarski and epifluorescence optics was used and the images acquisition were acquired with a Hamamatsu ORCA ER digital camera driven by Metamorph software (Universal Imaging Corporation), using Semrock Brightline GFP- 3035B and TXRED-4040B (mCherry) filter sets. Images were processed to a minimum using Metamorph (Universal Imaging Corporation) or ImageJ (http://rsb.info.nih.gov/ij/index.html) software.

Figure legends

Fig. 1. Effect of different extracellular concentrations of magnesium and calcium in *A. nidulans* mutants. Conidia from selected strains were point inoculated on AMM supplemented with the indicated concentrations of cations. Images were taken after 2 days of incubation at 37°C.

A. Effects of separate or mixed high concentrations of calcium and magnesium on the colonial growth of wild type and null *crzA* and *sltA* mutants.

B. Selected wild-type, *crzAΔ* and *sltAΔ* mutant strains were grown on AMM lacking any source for Mg^{2+} and the same minimal medium supplemented with the indicated amounts of Mg^{2+}.

Fig. 2. Phenotypic analysis of strains lacking a functional calcium channel and CrzA function.

Strains combining null alleles in *crzA* and of genes coding for the subunits of the calcium channel, *midA* and *cchA*, were analyzed for the sensitivity to different concentrations of calcium and the cross effect of adding magnesium. Conidia from each strain were point inoculated onto AMM supplemented with the indicated concentrations of calcium and magnesium.

709 Fig. 3. Effect of calcium and magnesium on the phosphorylation levels of CrzA.

710 A. Representative Western blots showing changes in the mobility of CrzA-GFP fusion in total
711 protein extracts from strain MAD3020 when subjected to treatments with a low (1 mM) and a
712 high (100 mM) concentration of calcium (Ca^{2+}). $CrzA^{+P}$ indicate highly phosphorylated forms of
713 CrzA, which had a reduced electrophoretic mobility. $CrzA^{-P}$ indicate non or very low
714 phosphorylated forms of CrzA, which had a higher electrophoretic mobility. Below are shown
715 lambda protein phosphatase (λPP) treatments of protein extract from RC to demonstrate that
716 the change in electrophoretic mobility of $CrzA^{+P}$ and $CrzA^{-P}$ forms depends on its
717 phosphorylated state.

718 B. Detection of CrzA-GFP fusion in protein extracts of cells subjected to treatment with
719 magnesium (Mg^{2+}) during the indicated times (in minutes).

720 C. Detection of CrzA-GFP in protein extracts of cells pretreated for 30 min with 100 mM Mg^{2+}
721 (RC30) and then supplemented with either 1 mM or 100 mM Ca^{2+} for the indicated times in
722 minutes.

723 RC indicates control protein extracts from resting cells.. $CrzA^{+P}$ indicates phosphorylated forms
724 of CrzA. $CrzA^{-P}$ indicates dephosphorylated or low phosphorylated forms of CrzA.

725

726 Fig. 4. Cellular distribution of CrzA-GFP in response to extracellular calcium and magnesium.

727 A. Chart depicting the dynamics of nuclear accumulation of the fluorescent protein CrzA-GFP in
728 response to 1 mM calcium (light grey bars), 100 mM calcium (dark grey bars) and 200 mM
729 magnesium (white bars) at different times over 30 min.

730 B. Chart showing the effect in nuclear accumulation of CrzA by combining 200 mM magnesium
731 plus 1 mM (striped bars) or 100 mM of calcium (dotted bars). For both panels, fluorescence
732 was measured inside 30 nuclei and in nearby cytoplasmic regions for 10 cell compartments (3
733 nuclei/compartment). Error bars indicate the standard error of the mean.

734

735

736 Fig. 5. Inhibition of CN activity by cyclosporin A suppresses CrzA-dependent sensitivity to Ca^{2+}.

737 A. Strains carrying single null *sltA* and *crzA* alleles and combination of null alleles of genes
738 coding for calcium channel subunits *cchA* and *midA* in a null *crzA* background were analyzed
739 for sensitivity to calcium in the absence or presence of calcineurin inhibitor cyclosporin A
740 (CsA). Each well contained 1 ml of AMM with the supplemented concentration of calcium
741 and/or CsA. For comparison, on the right (red square), the effect of 100 mM and 200 mM Mg^{2+}
742 on the growth of null *crzA* strain on medium containing 100 mM Ca^{2+} is shown. 10^3 conidia per
743 well were inoculated. Colonial growth was evaluated after 2 days of incubation at 37°C.

744 B. Quantitative analysis of suppression by CsA of calcium-sensitive phenotype of null *crzA*
745 strains. Mycelial growth was quantified from liquid AMM cultures in the same conditions as in
746 panel A. 10 ml of liquid AMM plus supplements were inoculated with 10^6 conidia/ml and
747 incubated at 37°C for 24 hr in liquid medium. Mycelia were filtered, dried and weighted.
748 Triplicates were done for each conditions and the mean weight values are shown. Standard
749 errors of the mean are indicated.

750

751 Fig. 6. Effect of *cnaB2* mutation.

752 A. Growth tests showing the suppression by *cnaB2* mutation of the calcium-sensitive
753 phenotype caused by the absence of CrzA function. Strains carrying an endogenous wild-type
754 *crzA* allele or carrying the *cnaB2* mutation tolerate the presence of calcium. Strains shown
755 were grown on AMM without or with supplementation of 50 mM calcium. Strains were point
756 inoculated and imaged after 2 days of incubation at 37°C.

757 B. Immunoblot showing the range of electrophoretic mobility displayed by the GFP-CrzA(1-
758 488) form in different genetic backgrounds. Detection of low mobility bands indicate the
759 presence of highly phosphorylated forms of CrzA

C. Immunodetection of GFP-CrzA(1-448) in protein extracts from resting cells of strains MAD2172, MAD5514 and MAD2168 treated with lambda protein phosphatase (λPP). The increase in electrophoretic mobility of GFP-CrzA(1-448) in extracts from MAD5514 and MAD2168 after treatment with λPP indicate the presence of phosphorylated forms in RCs of these strains but not in MAD2172.

Strains used are indicated at the bottom and genotypes are listed in Table 2. RC, resting/unstressed cells. CsA, calcineurin inhibitor cyclosporin A.

Fig. 7. Phosphoproteomics of CrzA.

A. Schematic drawing of the CrzA protein indicating the boundaries of the two truncated constructs used in the determination of phosphorylated peptides. The initial position of the main identified phosphopeptides is indicated with red arrows. Below are indicated the sequences of the phosphopeptides identified in the protein extracts of the *cnaB2* mutant strain expressing the GFP-CrzA(1-448) chimera, and of the strains expressing the GFP-CrzA(1-612) form with or without the calcineurin function. In red are indicated those serine residues potentially phosphorylated in CrzA.

B. CrzA amino acid sequence on which is indicated the position of identified phosphopeptides (overlaid in red), the ending coordinates of the truncated forms, the DNA binding domain (in yellow) and the calcineurin binding sequences. Green indicates the calcineurin docking site 1, CDD1, and blue indicates the CDD2 site that was shown to be the most functional (Hernández-Ortiz and Espeso, 2013).

Fig. 8. Transcriptional regulation of calcineurin regulator *rcnA*.

Northern blot showing expression levels of *rcnA* transcript in wild-type and *crzAΔ* strains grown in AMM with different concentrations of calcium and/or magnesium. Control indicates total RNA extracted from mycelia grown in standard AMM. $-Mg^{2+}$ indicates AMM lacking

786 magnesium salts. Calcium and magnesium chloride salts were added and mycelia samples
787 were collected after 10 min incubation. A 1.5 kbps fragment was used as a probe for *rcnA*
788 transcript. rRNA was used as loading control. At the bottom are shown the ratio of *rcnA* levels
789 vs intensity of 18S rRNA.
790
791 Fig. 9. Model of regulation of CN activity in *Aspergillus nidulans*. The key for each element in
792 this calcium signaling/regulatory pathway is shown.
793
794
795 Supporting information
796
797 Fig. S1. Immuno and epi-fluorescence detection of calcineurin regulatory subunit.
798 A. Immunoblots showing the mobility of CnaB-GFP fusion in protein extracts of mycelia grown
799 under non-stressing conditions (RC) and in time course experiments in which cultures were
800 supplemented with elevated concentrations of calcium and magnesium or alkalinized to pH 8.
801 B. Fluorescence microscopy of strain MAD5501 under non-stressing conditions. White
802 arrowheads point to the septa at which CN regulatory subunit accumulates at both sides.
803 Green arrowheads indicate cytoplasmic accretion of CnaB-GFP. Addition of calcium,
804 magnesium or alkalinization of medium did not modified these foci.
805
806 Fig. S2. Strategy of gene targeting.
807 Generation of null alleles and tagged versions of target genes follow the procedures described
808 in (Nayak *et al.*, 2006; Markina-Iñarrairaegui *et al.*, 2011). The figure describes the essential
809 steps for production of recombinant loci.
810 A. Strategy for deleting the CDS of a target gene. 5'UTR and 3'UTR regions were amplified with
811 specific primers. In the figure are indicated as nnn + plus a code for the gene specific primer

(GSP), where nnn refers to the target gene as indicated in the list of oligonucleotides. These two fragments were fused to a selectable cassette containing 5'UTR-CDS-3'UTR sequences of a selectable marker (SM), namely genes *riboB* or *pyrG* from *A. fumigatus*. Using PCR techniques and flanking oligonucleotides a transformation cassette was amplified by fusing the three fragments in the correct order. The cassette was used to transform protoplasts and those transformants with a double recombination event at the desired locus were selected, replacing the target gene by the selectable marker.

B. Strategy for epitope tagging of a target gene. As before a transformation cassette was generated by fusion PCR, using a fragment of the 3'end of CDS of target gene, the 3'UTR and a fragment containing the coding region for the tag, and the selectable marker. The cassette was used to transform protoplasts and those transformants with a double recombination event at the desired locus were selected, placing the tag on frame at the 3'end of the target gene followed by the selectable marker.

Table S1. Phosphoproteomic analysis of CrzA and control proteins PmaA and MepA in total protein extracts of RCs from strains MAD5513, MAD5514, MAD3494 and MAD3559.

829

Table 1: List of *Aspergillus nidulans* strains used in this work		
Strains	**Full Genotype**	**Sources**
MAD1425	*pyrG89, argB2; pyroA4, nkuAΔ::argB*	Markina-Inarrairaegui *et al.*, 2011
MAD1427	*pyrG89, pabaB22; argB2; nkuAΔ::argB, riboB2*	Markina-Inarrairaegui *et al.*, 2011
MAD2168	*pyrG89; argB2; pyroA*::gpdA^{m}::gfp::crzA(1-448), nkuAΔ::argB*	Hernández-Ortiz and Espeso, 2013
MAD2172	*pyrG89, yA2; arg*::afp::lacZ; pyroA*:: gpdA^{m}::gfp::crzA(1-448), nkuAΔ::argB; crzAΔ::pyr4^{Nc}; pantoB100*	Hernández-Ortiz and Espeso, 2013
MAD2666	*argB2; pyroA4, nkuAΔ::argB*	Garzia et al., 2013
MAD2448/ BER02	*pyrG89; argB2; pyroA4, nkuAΔ::argB; crzAΔ:: pyr4^{Nc}*	Spielvogel et al., 2008
MAD2740	*pyrG89, pabaB22; argB2, midAΔ::riboB^{Af}; nkuAΔ::argB; riboB2*	This work
MAD2741	*pyrG89, pabaB22; argB2; nkuAΔ::argB; cchAΔ::riboB^{Af}, riboB2*	This work
MAD2742	*pyrG89, pabaB22; argB2, midAΔ::riboB^{Af}; nkuAΔ::argB; cchAΔ:: pyrG^{Af} , riboB2*	This work
MAD2842	*pyrG89, pabaB22; argB2; nkuAΔ::argB; crzAΔ:: pyrG^{Af}; riboB2*	This work
MAD2843	*pyrG89, pabaB22; argB2, midAΔ::riboB^{Af}; nkuAΔ::argB; crzAΔ:: pyrG^{Af}; riboB2*	This work
MAD2844	*pyrG89, pabaB22; argB2; nkuAΔ::argB; crzAΔ:: pyrG^{Af}; cchAΔ:: riboB^{Af} , riboB2*	This work
MAD3020	*pyrG89, pabaB22; argB2, nkuAΔ::argB; crzA::gfp::pyrG^{Af}, riboB2*	Hernández-Ortiz and Espeso, 2013
MAD3021	*pyrG89, pabaB22; argB2, nkuAΔ::argB; crzA::gfp::pyrG^{Af}*	Hernández-Ortiz and Espeso, 2013
MAD3222	*pyrG89, pabaB22; cnaAΔ::pyroA, pyroA4 crzA::gfp::pyrG^{Af}*	Hernández-Ortiz and Espeso, 2013
MAD3709	*pyrG89, pabaB22; argB2; nkuAΔ::argB; crzAΔ::riboB^{Af}; riboB2*	Hernández-Ortiz and Espeso, 2013
MAD4096/ HHF27a	Prototrophic wild type	Findon et al., 2010
MAD4097/ HHF27b	*sltAΔ::riboB^{Af}*	Findon et al., 2010
MAD4100/ HHF27L	*crzAΔ::pyr4^{Nc}*	Sebastián et al., 2016
MAD5501	*pyrG89, cnaB-gfp-pyrG^{Af}; argB2; pyroA4, nkuAΔ::argB*	This work
MAD5507	*pyrG89, cnaB-gfp-pyrG^{Af}, pabaB22; argB2; nkuAΔ::argB; crzAΔ::riboB^{Af}; riboB2*	This work
MAD5513	*pyrG89; yA2; argB2 [argB*::afp::lacZ]; pyroA*::[pyroA*:: gpdA^{m}::gfp::crzA (M1-R448)], nkuAΔ::argB; crzAΔ::riboB^{Af}; riboB2; pantoB100*	This work
MAD5514	*cnaB2-HA::pyrG^{Af}; pyrG89; yA2; argB2 [argB*::afp::lacZ]; pyroA*::[pyroA*:: gpdA^{m}::gfp::crzA (M1-R448)], nkuAΔ::argB; crzAΔ::riboB^{Af}; riboB2; pantoB100*	This work
MAD5537/ rev-2	*crzAΔ::pyr4; cnaB2; paba-; wA3*	Almeida et al., 2013

830
831
832

Table 2: List of oligonucleotides used in this work			
Name	**Sequence 5´-3´**	**Description**	**Source**
CchA–PP1	ATCCCAACATGAGAATGCC	Generation of null *cchA* allele	This work
CchA–PP2	GGTGGGCAGAATTGATTGACTAGC	Generation of null *cchA* allele	This work
CchA–GSP3	ATAAAGCGCCGCTGAAGTGAGACG	Generation of null *cchA* allele	This work
CchA–GSP4	CGACTGTGGCTGTACTACACC	Generation of null *cchA* allele	This work
CchA–SMP	GCTAGTCAATCAATTCTGCCCACCACCGGTCGCCTCAAACAATGC	Generation of null *cchA* allele	This work
CchA–GSP3’	CGTCTCACTTCAGCGGCGCTTTATCTGTCTGAGAGGAGGCACTGATGC	Generation of null *cchA* allele	This work
cnaB fw_ol1	TGTCTCATTGCTTTTAGGTC	Sequencing *cnaB* allele	This work
cnaB rv_ol2	CGGACATACAGTTAGACCCGG	Sequencing *cnaB* allele	This work
cnaB-PP1	AGTATCCGCTCTGTCGCCAGCATCTCCTTTCGC	Generation of labeled CnaB	This work
cnaB-GSP2	AATTTGGTCTAATATCGCCGCATGTTAGC	Generation of labeled CnaB	This work
cnaB-GFP1	GCTAACATGCGGCGATATTAGACCAAATTGGAGCTGGTGCAGGCGCTGGAGCC	Generation of labeled CnaB	This work
cnaB-GSP3'	GGTATCCCATTTACGTTGCGCTAGAAAGTCTGAGAGGAGGCACTGATGCG	Generation of labeled CnaB	This work
cnaB-GSP3	TTTCTAGCGCAACGTAAATGGGATACC	Generation of labeled CnaB	This work
cnaB-GSP4	GCAACTTGCAAGACGCACTATCGATTTGAGG	Generation of labeled CnaB	This work
MidA–PP1	CCAGGAGTCACGTGAGAAAG	Generation of null *midA* allele	This work
MidA –PP2	GGGAGGTCAAGTGCTCCG	Generation of null *midA* allele	This work
MidA –GSP3	TCCTTTTCAAACTCGTCTTCC	Generation of null *midA* allele	This work
MidA–GSP4	GCTCAGGATGCATGACACC	Generation of null *midA* allele	This work
MidA–SMP	CGGAGCACTTGACCTCCCACCGGTCGCCTCAAACAATGC	Generation of null *midA* allele	This work
MidA –GSP3’	GGAAGACGAGTTTGAAAAGGACTGTCTGAGAGGAGGCACTGATGCG	Generation of null *midA* allele	This work
pyrGAnsequp	CAGCCATCCCACTTCCAGCTTC	Amplification of *A.nidulans pyrG* gene	This work
pyrGAnseqdw	CTGGTAATACTATGCTGGCTGC	Amplification of *A.nidulans pyrG* gene	This work
rcnA-GSP1	GGAGGTTGCTTTCTTTGCTGTGTTCCTAGG	Amplification of *rcnA* gene	This work
rcnA-GSP2	AACCATCAACTCAACAGGCGGTCGAGCAG	Amplification of *rcnA* gene	This work

833

Bibliography:

Aiello D.P., Fu L., Miseta A., Bedwell D.M. (2002). Intracellular Glucose 1-Phosphate and Glucose 6-Phosphate Levels Modulate Ca^{2+} Homeostasis in *Saccharomyces cerevisiae*. Journal of Biological Chemistry, 277(48), 45751–45758.

Almeida R.S., Loss O., Colabardini A.C., Brown N.A., Bignell E., Savoldi M., *et al.* (2013). Genetic Bypass of *Aspergillus nidulans crzA* Function in Calcium Homeostasis. Genes|Genomes|Genetics, 3(7), 1129–1141.

Boeckstaens M., Llinares E., Vooren P. Van, Marini A.M. (2014). The TORC1 effector kinase Npr1 fine tunes the inherent activity of the Mep2 ammonium transport protein. Nature communications, 5, 3101.

Boulousis G., Tsougeni K., Ellinas K., Speliotis A., Tserepi A., Gogolides E. (2011). TiO_2 affinity chromatography microcolumn on Si substrates for phosphopeptide analysis. Procedia Engineering, 25, 717–720.

Clutterbuck A. (1993). *Aspergillus nidulans*, nuclear genes. In: Cold Spring Harbor Laboratory Press (pp. 371–384).

Cove D.J. (1966). The induction and repression of nitrate reductase in the fungus *Aspergillus nidulans*. Biochimica et Biophysica Acta (BBA) - Enzymology and Biological Oxidation, 113(1), 51–56.

Cui J., Kaandorp J.A. (2006). Mathematical modeling of calcium homeostasis in yeast cells. Cell Calcium, 39(4), 337–348.

Cui J., Kaandorp J.A., Ositelu O.O., Beaudry V., Knight A., Nanfack Y.F., Cunningham K.W. (2009). Simulating calcium influx and free calcium concentrations in yeast. Cell Calcium, 45(2), 123–132.

Cui J., Kaandorp J.A., Sloot P.M.A., Lloyd C.M., Filatov M. V. (2009). Calcium homeostasis and signaling in yeast cells and cardiac myocytes. FEMS Yeast Research, 9(8), 1137–1147.

Cunningham K.W. (2005). Calcium Signaling Networks in Yeast. In: J.W. Putney (Ed.), Calcium

Signaling, Second Edition (pp. 107–201). Florida, USA, USA: Taylor & Francis Group. CRC Press.

Cyert M.S. (2003). Calcineurin signaling in *Saccharomyces cerevisiae*: how yeast go crazy in response to stress. Biochemical and Biophysical Research Communications, 311(4), 1143–1150.

Cyert M.S., Philpott C.C. (2013). Regulation of Cation Balance in *Saccharomyces cerevisiae*. Genetics, 193(3), 677–713.

Espeso E.A. (2016). The CRaZy calcium cycle. In: Advances in Experimental Medicine and Biology (pp. 169–186).

Estrada E., Agostinis P., Vandenheede J.R., Goris J., Merlevede W., François J., *et al.* (1996). Phosphorylation of yeast plasma membrane H^+-ATPase by casein kinase I. Journal of Biological Chemistry, 271(50), 32064–32072.

Findon H., Calcagno-Pizarelli A.-M., Martínez J.L., Spielvogel A., Markina-Iñarrairaegui A., Indrakumar T., *et al.* (2010). Analysis of a novel calcium auxotrophy in *Aspergillus nidulans*. Fungal Genetics and Biology, 47(7), 647–655.

Garzia A., Etxebeste O., Herrero-Garcia E., Fischer R., Espeso E.A., Ugalde U. (2009). *Aspergillus nidulans* FlbE is an upstream developmental activator of conidiation functionally associated with the putative transcription factor FlbB. Molecular Microbiology, 71(1), 172–184.

Garzia A., Etxebeste O., Rodríguez-Romero J., Fischer R., Espeso E.A., Ugalde U. (2013). Transcriptional Changes in the Transition from Vegetative Cells to Asexual Development in the Model Fungus *Aspergillus nidulans*. Eukaryotic Cell, 12(2), 311–321.

Genesca L., Aubareda A., Fuentes J.J., Estivill X., la Luna S. De, Pérez-Riba M. (2003). Phosphorylation of calcipressin 1 increases its ability to inhibit calcineurin and decreases calcipressin half-life. Biochemical Journal, 374(2), 567–575.

Görlach J., Fox D.S., Cutler N.S., Cox G.M., Perfect J.R., Heitman J. (2000). Identification and characterization of a highly conserved calcineurin binding protein, CBP1/calcipressin, in *Cryptococcus neoformans*. The EMBO Journal, 19(14), 3618–3629.

887 Grabarek Z. (2011). Insights into modulation of calcium signaling by magnesium in calmodulin,
888 troponin C and related EF-hand proteins. Biochimica et Biophysica Acta (BBA) - Molecular Cell
889 Research, 1813(5), 913–921.
890 Grubbs R.D. (2002). Intracellular magnesium and magnesium buffering. BioMetals, 15(3), 251–
891 259.
892 Guerini D. (1997). Calcineurin: Not just a simple protein phosphatase. Biochemical and
893 Biophysical Research Communications, 235(2), 271–275.
894 Hernández-Ortiz P., Espeso E.A. (2013). Phospho-regulation and nucleocytoplasmic trafficking
895 of CrzA in response to calcium and alkaline-pH stress in *Aspergillus nidulans*. Molecular
896 Microbiology, 89(3), 532–551.
897 Hernández-Ortiz P., Espeso E.A. (2017). Spatiotemporal dynamics of the calcineurin target
898 CrzA. Cellular Signalling, 29168–180.
899 Hirayama S., Sugiura R., Lu Y., Maeda T., Kawagishi K., Yokoyama M., *et al.* (2003). Zinc finger
900 protein Prz1 regulates Ca^{2+} but not Cl^{-} homeostasis in fission yeast. Identification of distinct
901 branches of calcineurin signaling pathway in fission yeast. Journal of Biological Chemistry,
902 278(20), 18078–18084.
903 Hu Z., Killion P.J., Iyer V.R. (2007). Genetic reconstruction of a functional transcriptional
904 regulatory network. Nature Genetics, 39(5), 683–687.
905 Käll L., Canterbury J.D., Weston J., Noble W.S., MacCoss M.J. (2007). Semi-supervised learning
906 for peptide identification from shotgun proteomics datasets. Nature Methods, 4(11), 923–925.
907 Karababa M., Valentino E., Pardini G., Coste A.T., Bille J., Sanglard D. (2006). CRZ1 , a target of
908 the calcineurin pathway in *Candida albicans*. Molecular Microbiology, 59(5), 1429–1451.
909 Kingsbury T.J., Cunningham K.W. (2000). A conserved family of calcineurin regulators. Genes
910 and Development, 14(13), 1595–1604.
911 Markina-Iñarrairaegui A., Etxebeste O., Herrero-García E., Araújo-Bazán L., Fernández-Martínez
912 J., Flores J.A., *et al.* (2011). Nuclear transporters in a multinucleated organism: functional and

913 localization analyses in *Aspergillus nidulans*. Molecular Biology of the Cell, 22(20), 3874–3886.
914 Mehta S., Li H., Hogan P.G., Cunningham K.W. (2009). Domain Architecture of the Regulators
915 of Calcineurin (RCANs) and Identification of a Divergent RCAN in Yeast. Molecular and Cellular
916 Biology, 29(10), 2777–2793.
917 Mellado L., Arst H.N., Espeso E.A. (2016). Proteolytic activation of both components of the
918 cation stress-responsive Slt pathway in *Aspergillus nidulans*. Molecular Biology of the Cell,
919 27(16), 2598–2612.
920 Mellado L., Calcagno-Pizarelli A.M., Lockington R.A., Cortese M.S., Kelly J.M., Arst H.N., Espeso
921 E.A. (2015). A second component of the SltA-dependent cation tolerance pathway in
922 *Aspergillus nidulans*. Fungal Genetics and Biology, 82116–128.
923 Mendizabal I., Pascual-Ahuir A., Serrano R., Larrinoa I.F. De (2001). Promoter sequences
924 regulated by the calcineurin-activated transcription factor Crz1 in the yeast ENA1 gene.
925 Molecular Genetics and Genomics, 265(5), 801–811.
926 Monahan B.J., Fraser J.A., Hynes M.J., Davis M.A. (2002). Isolation and characterization of two
927 ammonium permease genes, meaA and mepA, from *Aspergillus nidulans*. Eukaryotic Cell, 1(1),
928 85–94.
929 Nayak T., Szewczyk E., Oakley C.E., Osmani A., Ukil L., Murray S.L., *et al.* (2006). A versatile and
930 efficient gene-targeting system for *Aspergillus nidulans*. Genetics, 172(3), 1557–1566.
931 Ohki S.Y., Ikura M., Zhang M. (1997). Identification of Mg^{2+}-binding sites and the role of Mg^{2+}on
932 target recognition by calmodulin. Biochemistry, 36(14), 4309–4316.
933 Peñalva M.A. (2005). Tracing the endocytic pathway of *Aspergillus nidulans* with FM4-64.
934 Fungal Genetics and Biology, 42(12), 963–975.
935 Rappsilber J., Mann M., Ishihama Y. (2007). Protocol for micro-purification, enrichment, pre-
936 fractionation and storage of peptides for proteomics using StageTips. Nature Protocols, 2(8),
937 1896–1906.
938 Reoyo E., Espeso E.A., Peñalva M.A., Suárez T. (1998). The essential *Aspergillus nidulans* gene

939 *pmaA* encodes an homologue of fungal plasma membrane H^+-ATPases. Fungal Genetics and
940 Biology, 23(3), 288–299.
941 Sambrook J., Fritsch E.F., Maniatis T. (1989). Molecular Cloning, A Laboratory Manual (Second
942 Edition). New York: Cold Spring Harbor Laboratory Press.
943 Sebastián-Pérez V., Manoli M.-T., Pérez D.I., Gil C., Mellado E., Martínez A., *et al.* (2016). New
944 applications for known drugs: Human glycogen synthase kinase 3 inhibitors as modulators of
945 *Aspergillus fumigatus* growth. European Journal of Medicinal Chemistry, 116281–289.
946 Soriani F.M., Malavazi I., Silva Ferreira M.E. da, Savoldi M., Zeska Kress M.R. Von, Souza
947 Goldman M.H. de, *et al.* (2008). Functional characterization of the *Aspergillus fumigatus* CRZ1
948 homologue, CrzA. Molecular Microbiology, 67(6), 1274–1291.
949 Spielvogel A., Findon H., Arst H.N., Araújo-Bazán L., Hernández-Ortíz P., Stahl U., *et al.* (2008).
950 Two zinc finger transcription factors, CrzA and SltA, are involved in cation homoeostasis and
951 detoxification in *Aspergillus nidulans*. Biochemical Journal, 414(3), 419–429.
952 Tilburn J., Scazzocchio C., Taylor G.G., Zabicky-Zissman J.H., Lockington R.A., Davies R.W.
953 (1983). Transformation by integration in *Aspergillus nidulans*. Gene, 26(2–3), 205–221.
954 Tisi R., Rigamonti M., Groppi S., Belotti F. (2016). Calcium homeostasis and signaling in fungi
955 and their relevance forpathogenicity of yeasts and filamentous fungi. AIMS Molecular Science,
956 3(4), 505–549.
957 Wang S., Cao J., Liu X., Hu H., Shi J., Zhang S., *et al.* (2012). Putative Calcium Channels CchA and
958 MidA Play the Important Roles in Conidiation, Hyphal Polarity and Cell Wall Components in
959 *Aspergillus nidulans*. PLoS ONE, 7(10), e46564.
960 Wiesenberger G., Steinleitner K., Malli R., Graier W.F., Vormann J., Schweyen R.J., Stadler J.A.
961 (2007). Mg^{2+} deprivation elicits rapid Ca2+ uptake and activates Ca^{2+}/calcineurin signaling in
962 *Saccharomyces cerevisiae*. Eukaryotic Cell, 6(4), 592–599.
963 Wolf F.I., Trapani V. (2008). Cell (patho)physiology of magnesium. Clinical Science, 114(1), 27–
964 35.

965 Zakrzewska A., Boorsma A., Brul S., Hellingwerf K.J., Klis F.M. (2005). Transcriptional Response
966 of *Saccharomyces cerevisiae* to the Plasma Membrane-Perturbing Compound Chitosan.
967 Eukaryotic Cell, 4(4), 703–715.
968
969

Figure 1

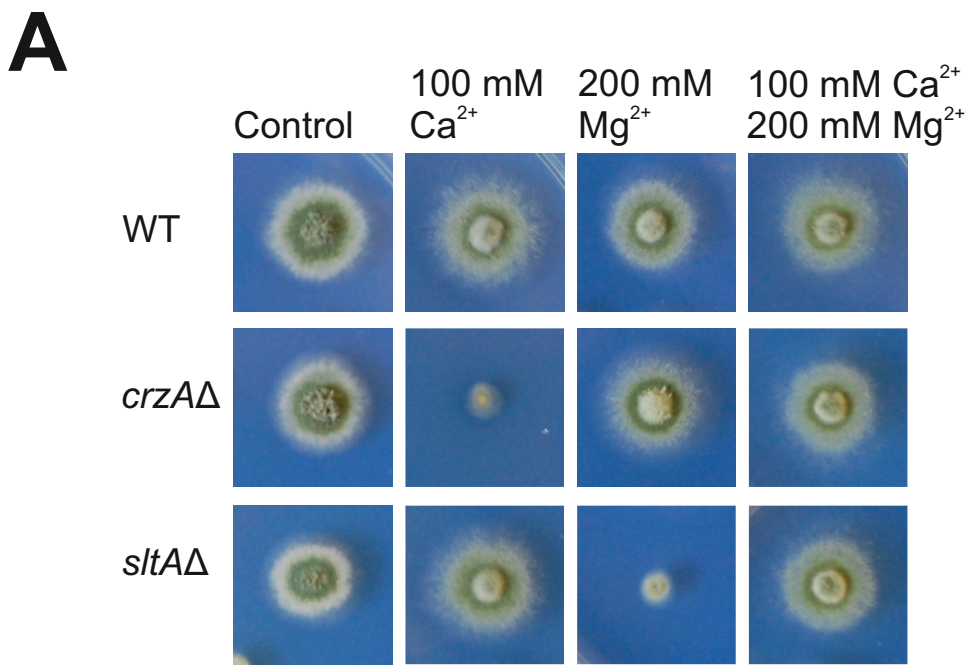
A
Control
100 mM Ca2+
200 mM Mg2+
100 mM Ca2+
200 mM Mg2+
WT
crzAΔ
sltAΔ
B
minus Mg2+
plus Mg2+ (mM)
0.02
0.2
1
5
WT
crzAΔ
sltAΔ

Figure 2

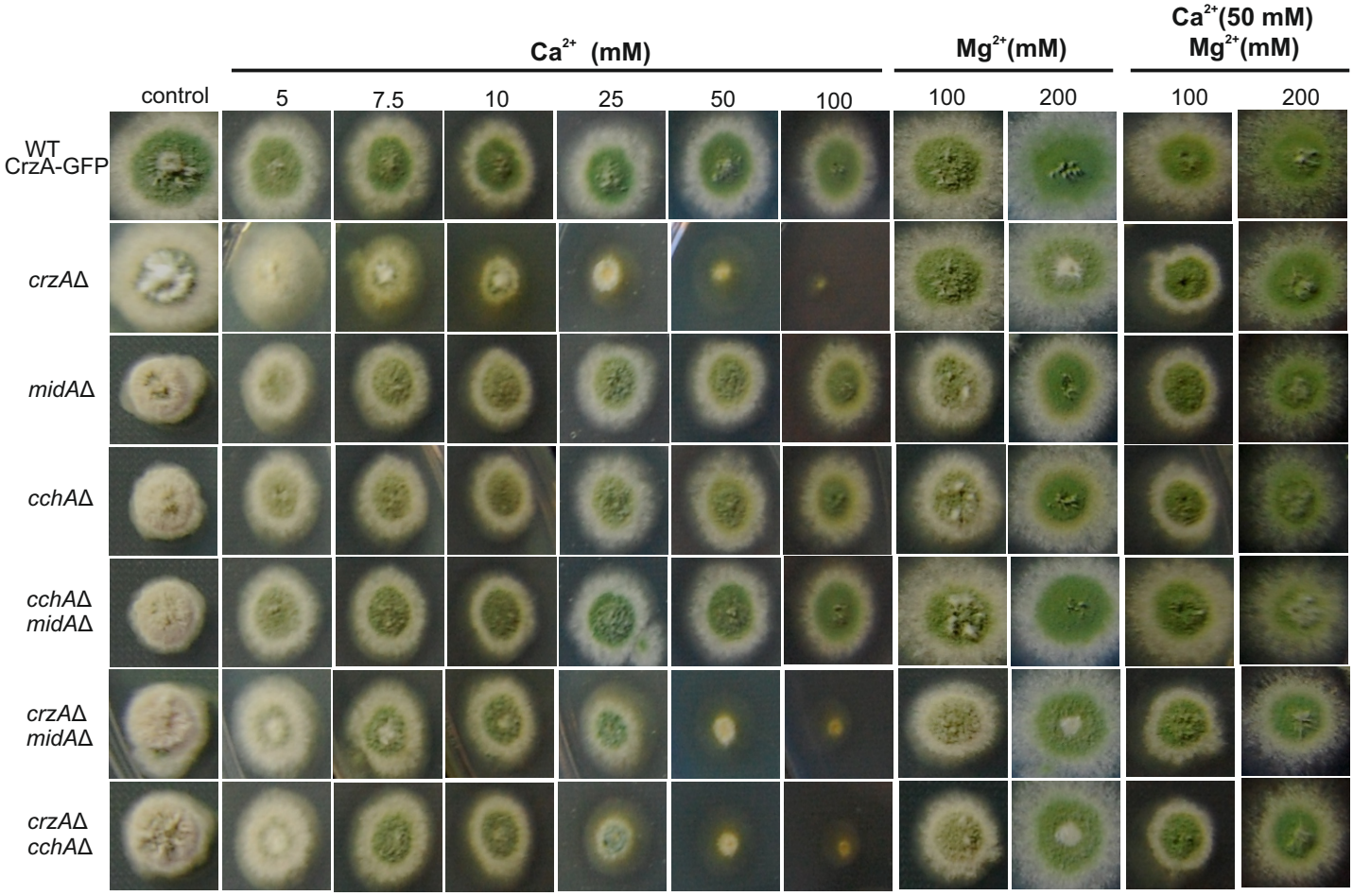
Ca2+ (mM)
Mg2+(mM)
Ca2+(50 mM)
Mg2+(mM)
control
5
7.5
10
25
50
100
100
200
100
200
WT
CrzA-GFP
crzAΔ
midAΔ
cchAΔ
cchAΔ
midAΔ
crzAΔ
midAΔ
crzAΔ
cchAΔ

Figure 3

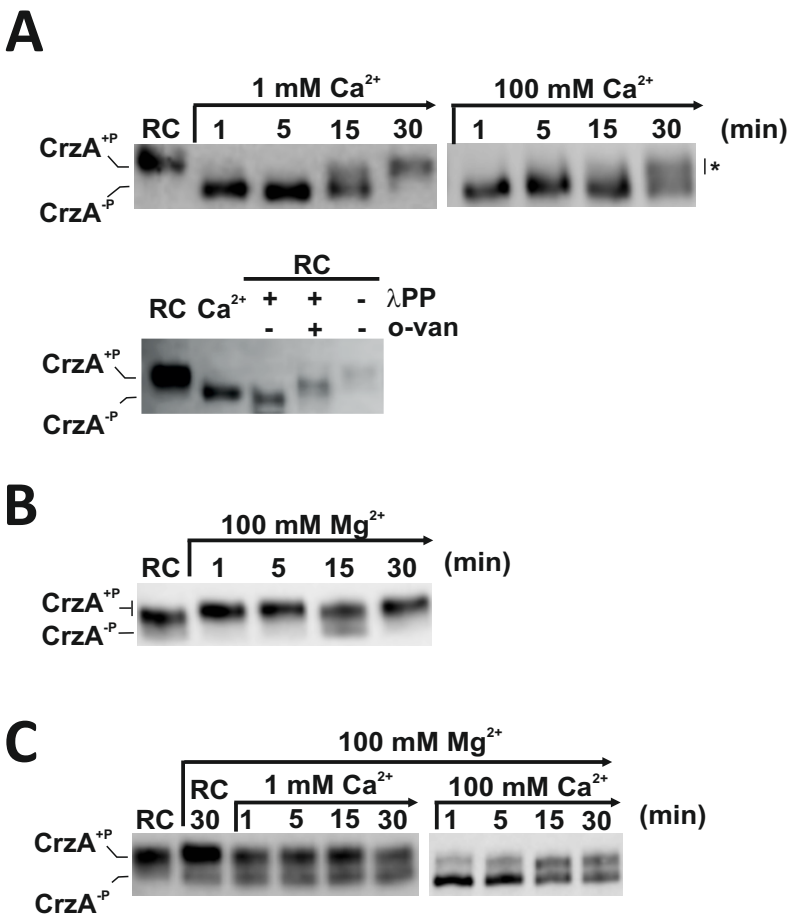
A
1 mM Ca2+
100 mM Ca2+
RC
1
5
15
30
1
5
15
30
(min)
CrzA+P
CrzA-P
*
RC
RC Ca2+
+
+
-
λPP
-
+
-
o-van
CrzA+P
CrzA-P
B
100 mM Mg2+
RC
1
5
15
30
(min)
CrzA+P
CrzA-P
C
100 mM Mg2+
RC
1 mM Ca2+
100 mM Ca2+
RC
30
1
5
15
30
1
5
15
30
(min)
CrzA+P
CrzA-P

Figure 4

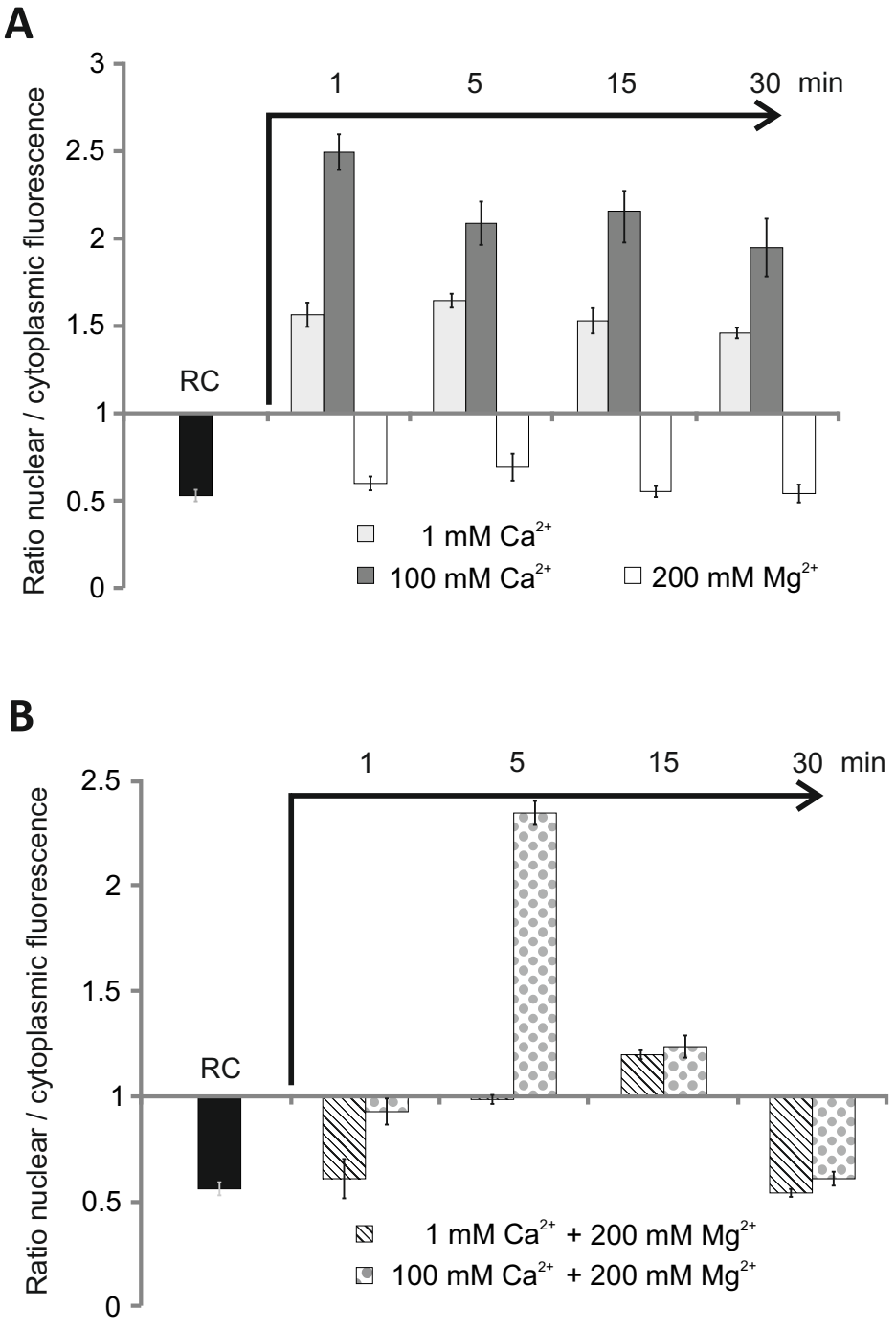
A
Ratio nuclear / cytoplasmic fluorescence
3
2.5
2
1.5
1
0.5
0
RC
1
5
15
30 min
1 mM Ca2+
100 mM Ca2+
200 mM Mg2+
B
Ratio nuclear / cytoplasmic fluorescence
2.5
2
1.5
1
0.5
0
RC
1
5
15
30 min
1 mM Ca2+ + 200 mM Mg2+
100 mM Ca2+ + 200 mM Mg2+

Figure 5

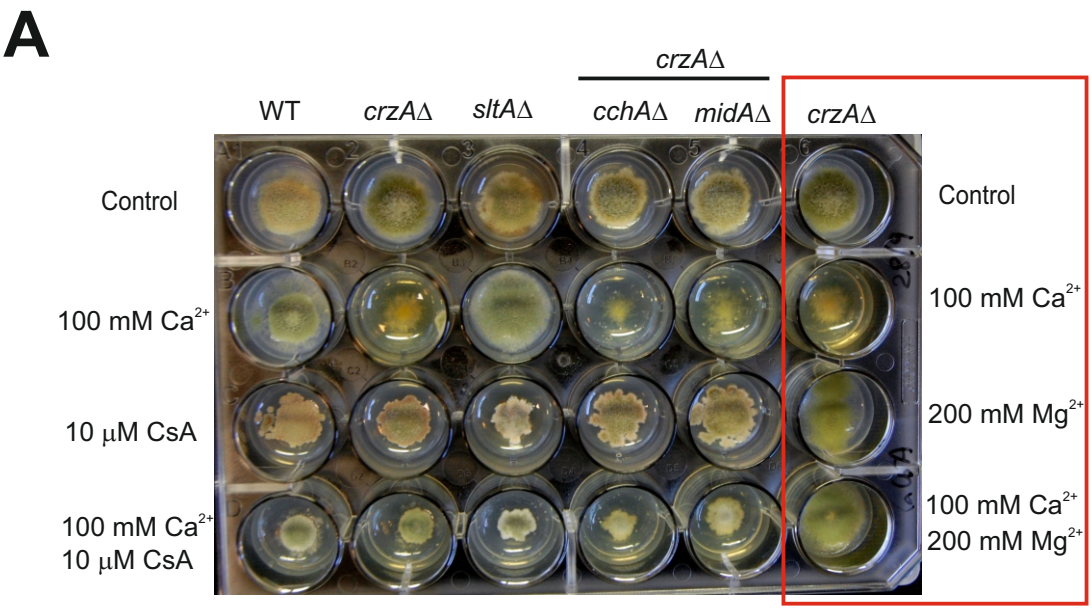
A
crzAΔ
WT
crzAΔ
sltAΔ
cchAΔ
midAΔ
crzAΔ
Control
100 mM Ca2+
10 μM CsA
100 mM Ca2+
10 μM CsA
Control
100 mM Ca2+
200 mM Mg2+
100 mM Ca2+
200 mM Mg2+

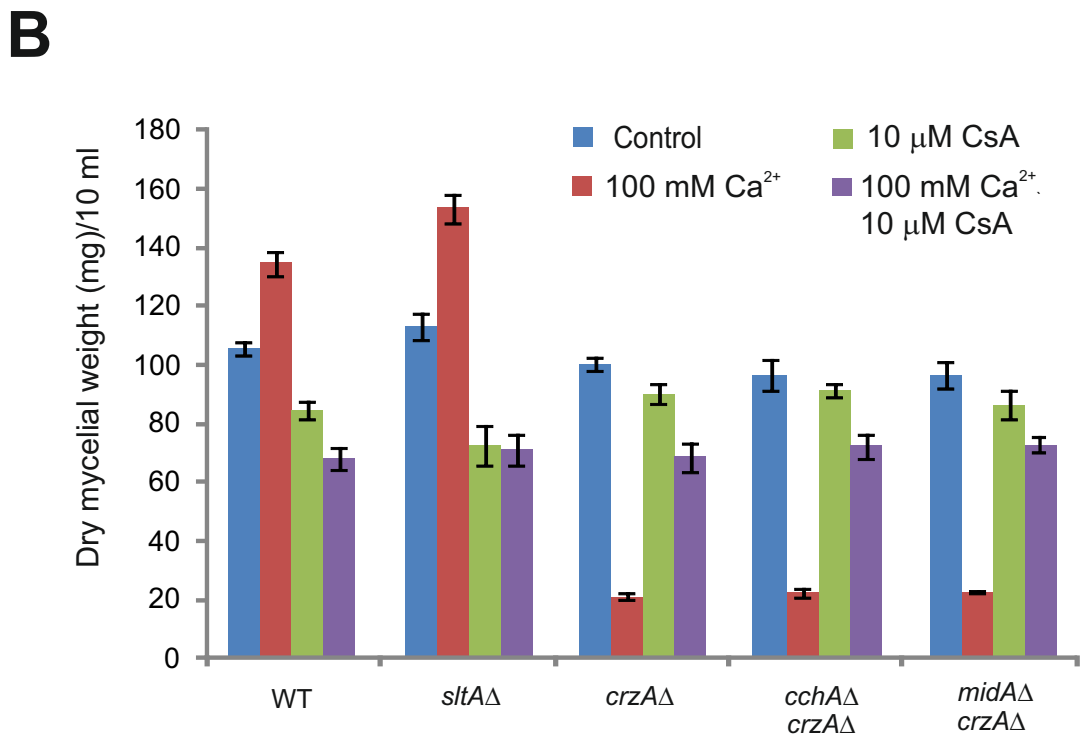
B
Dry mycelial weight (mg)/10 ml
180
160
140
120
100
80
60
40
20
0
Control
100 mM Ca2+
10 μM CsA
100 mM Ca2+
10 μM CsA
WT
sltAΔ
crzAΔ
cchAΔ crzAΔ
midAΔ crzAΔ

Figure 6

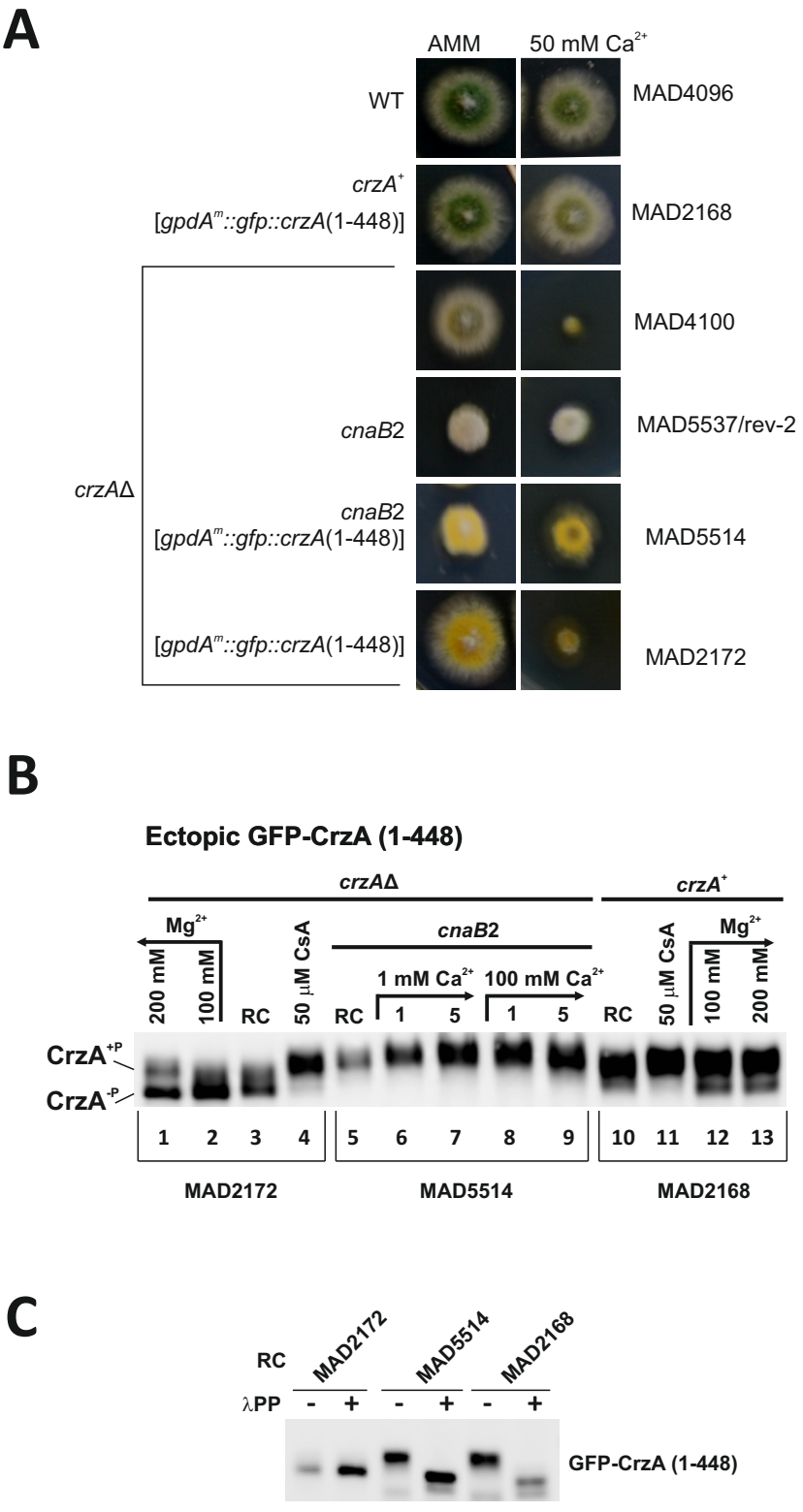
A
AMM
50 mM Ca2+
WT
MAD4096
crzA+
[gpdAm::gfp::crzA(1-448)]
MAD2168
crzAΔ
MAD4100
cnaB2
MAD5537/rev-2
cnaB2
[gpdAm::gfp::crzA(1-448)]
MAD5514
[gpdAm::gfp::crzA(1-448)]
MAD2172
B
Ectopic GFP-CrzA (1-448)
crzAΔ
crzA+
Mg2+
200 mM
100 mM
RC
50 μM CsA
cnaB2
1 mM Ca2+
100 mM Ca2+
1
5
1
5
RC
50 μM CsA
Mg2+
100 mM
200 mM
CrzA+P
CrzA-P
1 2 3 4 5 6 7 8 9 10 11 12 13
MAD2172
MAD5514
MAD2168
C
RC
MAD2172
MAD5514
MAD2168
λPP
- + - + - +
GFP-CrzA (1-448)

Figure 7

A

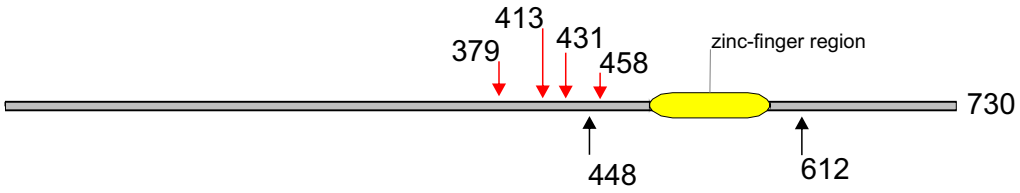

cnaB2 CrzA(1-448)
S_{413}PSSPSASLDALAASSPR S_{431}LSPFNVGR

cnaA+ CrzA(1-612)
S_{379}TADMDSLSPPPSLR
S_{413}PSSPSASLDALAASSPR S_{431}LSPFNVGR R_{458}LSTSSVDSR

*cnaA*Δ CrzA(1-612)
S_{379}TADMDSLSPPPSLR
S_{431}LSPFNVGR R_{458}LSTSSVDSR

B

```
  1  MDPQDTLQDL GQAPAAHINR SASPSAHAHQ QYNNNHNDLT IDPSVTSNSS
 51  YPPSSFANNS APGSEAFAYS SSYLTPATAT DHNFARPSLQ IPQSFDQGLS
101  HQPAEENFSN LLNSNTGDFD FSLYQGSSPN NTGSDYPSSG LLDPQQSGNQ
151  AVNPVDLVSQ IPSPHPSNSS QTSPLDQPPS SAMSPPASSP GTFYTPQHSR
201  HTSLDPASAA YMTNVSHPEW QAVMNNSAFH GHRRAPSEVS EVSSAAHSPY
251  LPQHDSFDVA DNNPSPLLAA QNDPSLYDNA ALGIESFTLS EHHQPQTQGI
301  SPHHSPYISP QLMPQHPTDI IPGGPFISAP ATNSAYPTPP TEGYPNGGDI
351  GQASQMAPPS INVEFAPPAK AQVFPPEKST ADMDSLSPPP SLRTSRMRSK
401  SDPYAVSISR PRSPSSPSAS LDALAASSPR SLSPFNVGRH PYSNPSSR ← 448
                                                       EP
451  SPARSARRLS TSSVDSRNYI LGLADPQRPG SNNTDSKRVQ KHPATFQCTL
501  CPKRFTRAYN LRSHLRTHTD ERPFVCTVCG KAFARQHDRK RHEGLHSGEK
551  KFVCRGDLSR GGQWGCGRRF ARADALGRHF RSEAGRICIK PLLDEESQER
601  ERTLINQQQQ HL ← 612
                 QPVNQPLM LPGQGTEAQH TGSFILPAAL LAQYPALQTL
651  QWDQIPAGTD DTSDIGGRNS FDASSGGEFG FDDDESGISV SGMSTGYASD
701  QGNIYNVDAQ GQMLGVNPGE AGYANPNWGK
```

Figure 8

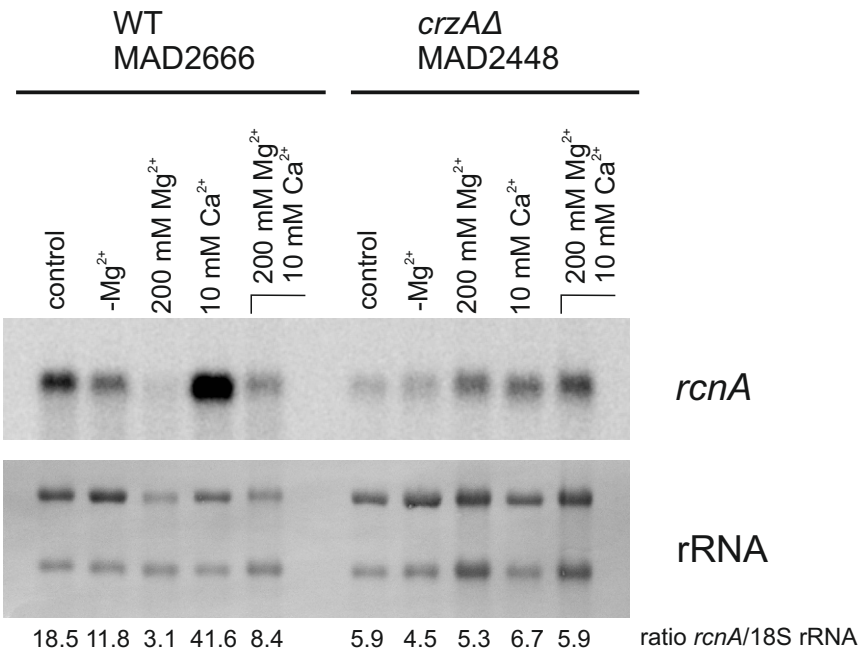
WT
MAD2666
crzAΔ
MAD2448
control
-Mg2+
200 mM Mg2+
10 mM Ca2+
200 mM Mg2+
10 mM Ca2+
control
-Mg2+
200 mM Mg2+
10 mM Ca2+
200 mM Mg2+
10 mM Ca2+
rcnA
rRNA
18.5 11.8 3.1 41.6 8.4
5.9 4.5 5.3 6.7 5.9
ratio rcnA/18S rRNA

Figure 9

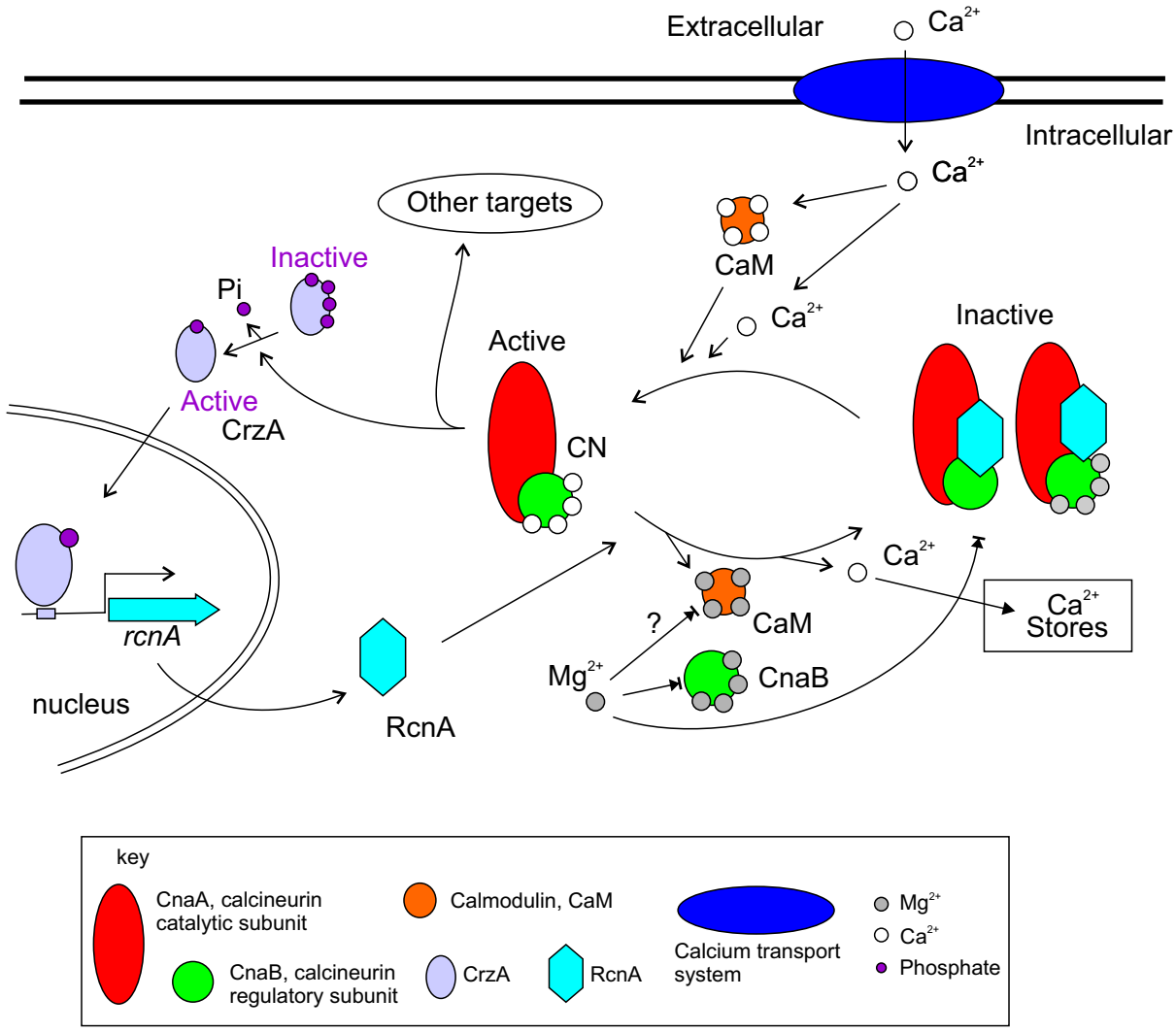
Extracellular
Ca2+
Intracellular
Ca2+
Other targets
CaM
Inactive
Pi
Ca2+
Active
Inactive
Active
CrzA
CN
rcnA
Ca2+
Ca2+
Stores
?
CaM
Mg2+
CnaB
nucleus
RcnA
key
CnaA, calcineurin catalytic subunit
Calmodulin, CaM
Calcium transport system
Mg2+
Ca2+
Phosphate
CnaB, calcineurin regulatory subunit
CrzA
RcnA

Fig. S1

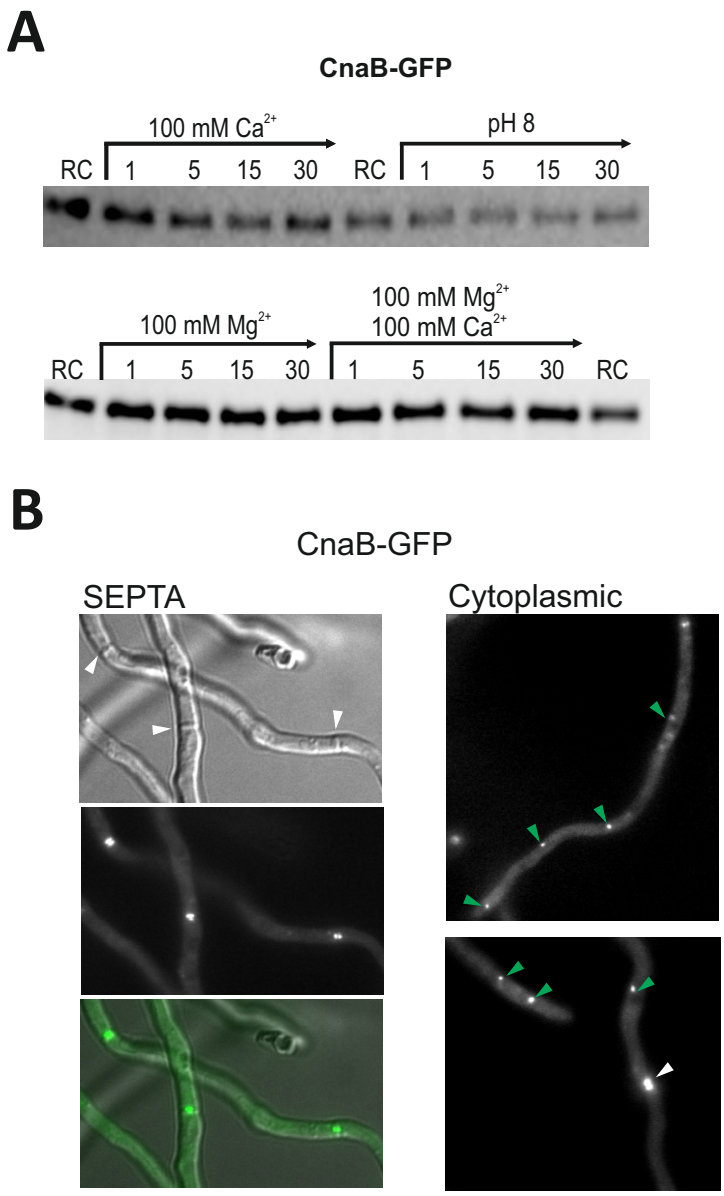

Fig. S1. Immuno and epi-fluorescence detection of calcineurin regulatory subunit.

A. Immunoblots showing the mobility of CnaB-GFP fusion in protein extracts of mycelia grown under non-stressing conditions (RC) and in time course experiments in which cultures were supplemented with elevated concentrations of calcium and magnesium or alkalinized to pH 8. B. Fluorescence microscopy of strain MAD5501 under non-stressing conditions. White arrowheads point to the septa at which CN regulatory subunit accumulates at both sides. Green arrowheads indicate cytoplasmic accretion of CnaB-GFP. Addition of calcium, magnesium or alkalinization of medium did not modified these foci.

Fig. S2

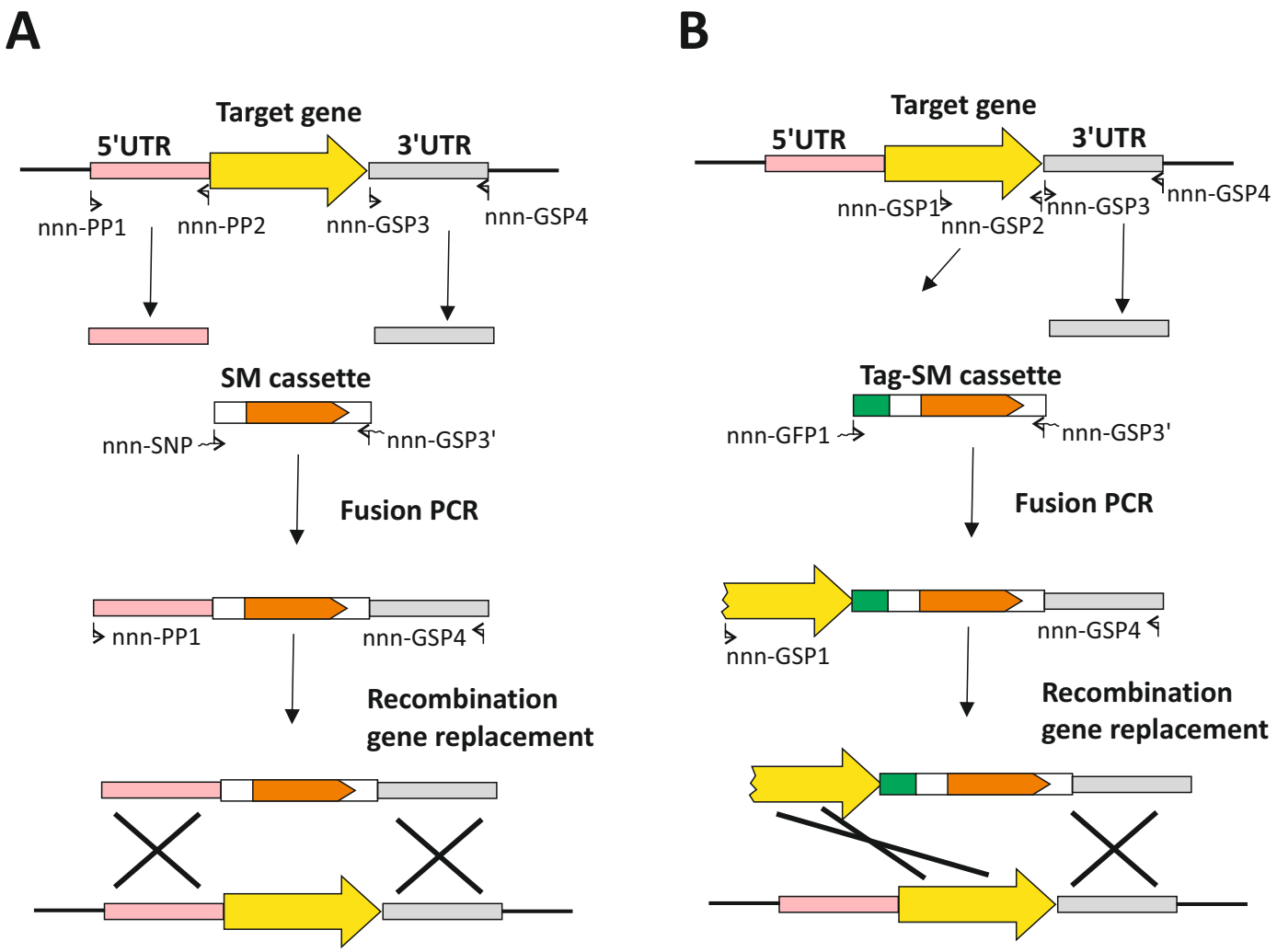

Fig. S2. Strategy of gene targeting.

Generation of null alleles and tagged versions of target genes follow the procedures described in (Nayak et al., 2006; Markina-Iñarrairaegui et al., 2011). The figure describes the essential steps for production of recombinant loci.

A. Strategy for deleting the CDS of a target gene. 5'UTR and 3'UTR regions were amplified with specific primers. In the figure are indicated as nnn + plus a code for the gene specific primer (GSP), where nnn refers to the target gene as indicated in the list of oligonucleotides. These two fragments were fused to a selectable cassette containing 5'UTR-CDS-3'UTR sequences of a selectable marker (SM), namely genes *riboB* or *pyrG* from *A. fumigatus*. Using PCR techniques and flanking oligonucleotides a transformation cassette was amplified by fusing the three fragments in the correct order. The cassette was used to transform protoplasts and those transformants with a double recombination event at the desired locus were selected, replacing the target gene by the selectable marker.

B. Strategy for epitope tagging of a target gene. As before a transformation cassette was generated by fusion PCR, using a fragment of the 3'end of CDS of target gene, the 3'UTR and a fragment containing the coding region for the tag, and the selectable marker. The cassette was used to transform protoplasts and those transformants with a double recombination event at the desired locus were selected, placing the tag on frame at the 3'end of the target gene followed by the selectable marker.

Table S1

MAD5513 Strain expressing CrzA(1-448)

Accession	Description	Score	Coverage	# Proteins	# Unique Peptides	# Peptides	# PSMs
AN5726							

CrzA, AN5726 Phospho-peptides not detected

Accession	Description	Score	Coverage	# Proteins	# Unique Peptides	# Peptides	# PSMs
AN1181	mepA AspGDID:A	34,74	3,77	1	3	3	19

Control 1

MepA, AN1181

A2	Sequence	# PSMs	# Proteins	# Protein Groups	Protein Group Accessions	Modifications
High	SttPTGPVEPSPAELKA	4	1	1	AN1181	T2(Phospho); T3(Phospho)
High	STtPTGPVEPSPAELKA	10	1	1	AN1181	T3(Phospho)
High	RSttPTGPVEPSPAELKA	3	1	1	AN1181	T3(Phospho); T4(Phospho)
High	SttPTGPVEPSPAELK	2	1	1	AN1181	T2(Phospho); T3(Phospho)

Control 2

PmaA, AN4859

Accession	Description	Score	Coverage	# Proteins	# Unique Peptides	# Peptides	# PSMs
AN4859	pmaA AspGDID:A	91,45	2,53	1	5	5	39

A2	Sequence	# PSMs	# Proteins	# Protein Groups	Protein Group Accessions	Modifications
High	RGsTsSAGALSMK	6	1	1	AN4859	S3(Phospho); S5(Phospho)
High	RGSTssAGALsMKQK	5	1	1	AN4859	S5(Phospho); S6(Phospho); S11(Phospho)
High	GSTSsAGALSMK	3	1	1	AN4859	S5(Phospho)
High	RGsTsSAGALSMk	7	1	1	AN4859	S3(Phospho); S5(Phospho); C-Term(Oxidation)
High	GSTSsAGALsMK	2	1	1	AN4859	S5(Phospho); S10(Phospho)
High	RGStSsAGALsMK	5	1	1	AN4859	T4(Phospho); S6(Phospho); S11(Phospho)
High	GSTSsAGALSMk	2	1	1	AN4859	S5(Phospho); C-Term(Oxidation)

High	RGStSsAGALsMk	1	1	1	AN4859	T4(Phospho); S6(Phospho); S11(Phospho); C-Term(Oxidation)
High	GSTSsAGALsMKQK	3	1	1	AN4859	S5(Phospho); S10(Phospho)
High	RGSTSsAGALsMKQK	2	1	1	AN4859	S6(Phospho); S11(Phospho)
High	GSTSsAGALsMk	1	1	1	AN4859	S5(Phospho); S10(Phospho); C-Term(Oxidation)
High	RGStSsAGALsMKQk	1	1	1	AN4859	T4(Phospho); S6(Phospho); S11(Phospho); C-Term(Oxidation)

MAD5514 *cnaB2* mutant expressing CrzA(1-448)

CrzA, AN5726

Accession	Description	Score	Coverage	# Proteins	# Unique Peptides	# Peptides	# PSMs
AN5726	crzA AspGDID:AS	25,60	3,70	1	2	2	13

A2	Sequence	# PSMs	# Proteins	# Protein Groups	Protein Group Accessions	Modifications
High	SPSSPsAsLDALAAsSPR	5	1	1	AN5726	S6(Phospho); S8(Phospho); S15(Phospho)
High	SPSSPSAsLDALAAsSPR	7	1	1	AN5726	S8(Phospho); S15(Phospho)
High	sLsPFNVGR	1	1	1	AN5726	S1(Phospho); S3(Phospho)

Control 1

MepA, AN1181

Accession	Description	Score	Coverage	# Proteins	# Unique Peptides	# Peptides	# PSMs
AN1181	mepA AspGDID:A	52,42	3,77	1	2	2	28

A2	Sequence	# PSMs	# Proteins	# Protein Groups	Protein Group Accessions	Modifications
High	SttPTGPVEPSPAELKA	8	1	1	AN1181	T2(Phospho); T3(Phospho)
High	RSttPTGPVEPSPAELKA	4	1	1	AN1181	T3(Phospho); T4(Phospho)
High	sTTPTGPVEPSPAELKA	16	1	1	AN1181	S1(Phospho)

Control 2

Accession	Description	Score	Coverage	# Proteins	# Unique Peptides	# Peptides	# PSMs
AN4859	pmaA AspGDID:A	33,00	2,83	1	5	5	15

PmaA, AN4859

A2	Sequence	# PSMs	# Proteins	# Protein Groups	Protein Group Accessions	Modifications
High	RGsTsSAGALSMK	5	1	1	AN4859	S3(Phospho); S5(Phospho)
High	GSTSSAGALsMK	2	1	1	AN4859	S10(Phospho)
High	GSTSsAGALsMK	1	1	1	AN4859	S5(Phospho); S10(Phospho)
High	RGSTSsAGALsMk	2	1	1	AN4859	S6(Phospho); S11(Phospho); C-Term(Oxidation)
High	RGSTssAGALsMKQK	3	1	1	AN4859	S5(Phospho); S6(Phospho); S11(Phospho)
High	DNRRGStSsAGALsMK	1	1	1	AN4859	T7(Phospho); S9(Phospho); S14(Phospho)

MAD3494 WT, strain expressing CrzA(1-612)

CrzA, AN5726

Accession	Description	Score	Coverage	# Proteins	# Unique Peptides	# Peptides	# PSMs
AN5726	crzA AspGDID:AS	42,74	7,12	1	4	4	22

A2	Sequence	# PSMs	# Proteins	# Protein Groups	Protein Group Accessions	Modifications
High	SPssPSASLDALAASSPR	14	1	1	AN5726	S3(Phospho); S4(Phospho)
High	STADMDSLsPPPsLR	2	1	1	AN5726	S9(Phospho); S13(Phospho)
High	RLsTSSVDSR	2	1	1	AN5726	S3(Phospho)
High	RLsTsSVDSR	2	1	1	AN5726	S3(Phospho); S5(Phospho)
High	SPSSPsAsLDALAAsSPR	1	1	1	AN5726	S6(Phospho); S8(Phospho); S15(Phospho)
High	sLsPFNVGR	1	1	1	AN5726	S1(Phospho); S3(Phospho)

Control 1

MepA, AN1181

Accession	Description	Score	Coverage	# Proteins	# Unique Peptides	# Peptides	# PSMs
AN1181	mepA AspGDID:A	49,98	3,77	1	2	2	28

A2	Sequence	# PSMs	# Proteins	# Protein Groups	Protein Group Accessions	Modifications
High	SttPTGPVEPSPAELKA	8	1	1	AN1181	T2(Phospho); T3(Phospho)
High	STtPTGPVEPSPAELKA	13	1	1	AN1181	T3(Phospho)
High	RSttPTGPVEPSPAELKA	7	1	1	AN1181	T3(Phospho); T4(Phospho)

Control 2

PmaA/AN4859

Accession	Description	Score	Coverage	# Proteins	# Unique Peptides	# Peptides	# PSMs
AN4859	pmaA AspGDID:A	133,17	2,83	1	6	6	59

A2	Sequence	# PSMs	# Proteins	# Protein Groups	Protein Group Accessions	Modifications
High	RGsTsSAGALSMK	6	1	1	AN4859	S3(Phospho); S5(Phospho)
High	GSTSsAGALsMK	2	1	1	AN4859	S5(Phospho); S10(Phospho)
High	RGStSsAGALsMK	5	1	1	AN4859	T4(Phospho); S6(Phospho); S11(Phospho)
High	RGsTsSAGALSMk	5	1	1	AN4859	S3(Phospho); S5(Phospho); C-Term(Oxidation)
High	RGsTssAGALSMk	2	1	1	AN4859	S3(Phospho); S5(Phospho); S6(Phospho); C-Term(Oxidation)
High	RGSTSsAGALsMKQK	3	1	1	AN4859	S6(Phospho); S11(Phospho)
High	RGsTSSAGALSMk	1	1	1	AN4859	S3(Phospho); C-Term(Oxidation)
High	GSTSSAGALsMK	2	1	1	AN4859	S10(Phospho)
High	GSTSsAGALsMKQK	2	1	1	AN4859	S5(Phospho); S10(Phospho)
High	GSTSSAGALsMk	3	1	1	AN4859	S10(Phospho); C-Term(Oxidation)
High	RGStSsAGALsMKQK	11	1	1	AN4859	T4(Phospho); S6(Phospho); S11(Phospho)
High	DNRRGsTssAGALSMK	4	1	1	AN4859	S6(Phospho); S8(Phospho); S9(Phospho)
High	GSTSsAGALsMk	2	1	1	AN4859	S5(Phospho); S10(Phospho); C-Term(Oxidation)
High	GStSsAGALsMKQK	2	1	1	AN4859	T3(Phospho); S5(Phospho); S10(Phospho)
High	RGStSsAGALsMKQk	4	1	1	AN4859	T4(Phospho); S6(Phospho); S11(Phospho); C-Term(Oxidation)
High	DNRRGsTsSAGALSMk	1	1	1	AN4859	S6(Phospho); S8(Phospho); C-Term(Oxidation)

High	GSTSsAGALsMKQk	1	1	1	AN4859	S5(Phospho); S10(Phospho); C-Term(Oxidation)
High	DNRRGsTsSAGALSMK	2	1	1	AN4859	S6(Phospho); S8(Phospho)

MAD3559 Null *cnaA* strain expressing CrzA(1-612)

CrzA, AN5726

Accession	Description	Score	Coverage	# Proteins	# Unique Peptides	# Peptides	# PSMs
AN5726	crzA AspGDID:AS	15,56	4,66	1	3	3	7

A2	Sequence	# PSMs	# Proteins	# Protein Groups	Protein Group Accessions	Modifications
High	RLsTssVDSR	1	1	1	AN5726	S3(Phospho); S5(Phospho); S6(Phospho)
High	RLsTsSVDSR	2	1	1	AN5726	S3(Phospho); S5(Phospho)
High	sLsPFNVGR	1	1	1	AN5726	S1(Phospho); S3(Phospho)
High	STADMDSLsPPPsLR	2	1	1	AN5726	S9(Phospho); S13(Phospho)
High	RLsTSSVDSR	1	1	1	AN5726	S3(Phospho)

Control 1

MepA, AN1181

Accession	Description	Score	Coverage	# Proteins	# Unique Peptides	# Peptides	# PSMs
AN1181	mepA AspGDID:A	42,56	3,77	1	2	2	22

A2	Sequence	# PSMs	# Proteins	# Protein Groups	Protein Group Accessions	Modifications
High	SttPTGPVEPSPAELKA	9	1	1	AN1181	T2(Phospho); T3(Phospho)
High	RSttPTGPVEPSPAELKA	6	1	1	AN1181	T3(Phospho); T4(Phospho)
High	STtPTGPVEPSPAELKA	7	1	1	AN1181	T3(Phospho)

Control 2

PmaA/AN4859

Accession	Description	Score	Coverage	# Proteins	# Unique Peptides	# Peptides	# PSMs
AN4859	pmaA AspGDID:A	70,42	3,43	1	7	7	38

A2	Sequence	# PSMs	# Proteins	# Protein Groups	Protein Group Accessions	Modifications
High	RGsTsSAGALSMK	3	1	1	AN4859	S3(Phospho); S5(Phospho)
High	RGStSsAGALsMK	3	1	1	AN4859	T4(Phospho); S6(Phospho); S11(Phospho)
High	GSTSsAGALsMK	1	1	1	AN4859	S5(Phospho); S10(Phospho)

	High	DNRRGStSsAGALsMK	2	1	1	AN4859	T7(Phospho); S9(Phospho); S14(Phospho)
	High	RGSTSsAGALsMk	4	1	1	AN4859	S6(Phospho); S11(Phospho); C-Term(Oxidation)
	High	RGStSsAGALsMk	1	1	1	AN4859	T4(Phospho); S6(Phospho); S11(Phospho); C-Term(Oxidation)
	High	GSTSsAGALSMK	1	1	1	AN4859	S5(Phospho)
	High	RGStSsAGALsMKQK	8	1	1	AN4859	T4(Phospho); S6(Phospho); S11(Phospho)
	High	GSTSsAGALsMKQK	2	1	1	AN4859	S5(Phospho); S10(Phospho)
	High	RGSTSsAGALSMk	1	1	1	AN4859	S6(Phospho); C-Term(Oxidation)
	High	DNRRGSTssAGALSMK	2	1	1	AN4859	S8(Phospho); S9(Phospho)
	High	DNRRGStSsAGALsMk	1	1	1	AN4859	T7(Phospho); S9(Phospho); S14(Phospho); C-Term(Oxidation)
	High	RGStSsAGALsMKQk	3	1	1	AN4859	T4(Phospho); S6(Phospho); S11(Phospho); C-Term(Oxidation)
	High	YIsTARDNR	1	1	1	AN4859	S3(Phospho)
	High	GSTSsAGALsMKQk	1	1	1	AN4859	S5(Phospho); S10(Phospho); C-Term(Oxidation)
	High	GSTSsAGALsMk	1	1	1	AN4859	S5(Phospho); S10(Phospho); C-Term(Oxidation)
	High	GStSsAGALsMKQK	2	1	1	AN4859	T3(Phospho); S5(Phospho); S10(Phospho)

Control MepA, Putative transporter with a predicted role in small molecule transport; ammonium permease

Monahan BJ, *et al.* (2002) Isolation and characterization of two ammonium permease genes, meaA and mepA, from Aspergillus nidulans

Control PmaA Plasma membrane ATPase with a predicted role in energy metabolism

Reoyo E, *et al.* (1998) The essential Aspergillus nidulans gene pmaA encodes an homologue of fungal plasma membrane H(+)-ATPases

# AAs	MW [kDa]	calc. pI

# AAs	MW [kDa]	calc. pI
478	51,1	5,60

ΔCn	q-Value	PEP	XCorr	Charge	MH+ [Da]	ΔM [ppm]	RT [min]	# Missed Cleavages
0,0000	0	2,348E-07	4,88	2	1841,80840	6,16	60,76	1
0,0000	0	0,00009695	3,74	2	1761,83721	3,68	53,55	1
0,0000	0	0,0002647	2,43	2	1997,90654	4,19	52,56	2
0,0000	0,002	0,01035	2,47	2	1770,77434	8,14	57,31	0

# AAs	MW [kDa]	calc. pI
990	108,7	5,36

ΔCn	q-Value	PEP	XCorr	Charge	MH+ [Da]	ΔM [ppm]	RT [min]	# Missed Cleavages
0,0000	0	0,00007717	3,94	2	1412,56816	2,85	38,84	1
0,0000	0	0,00006741	3,84	3	1748,68869	2,67	33,96	2
0,0000	0	0,00004378	3,82	2	1176,49944	2,33	39,49	0
0,0417	0	0,00007604	3,68	2	1428,56377	3,30	29,49	1
0,0000	0	0,0007897	3,51	2	1256,46721	3,33	44,20	0
0,0000	0	0,0002721	3,48	2	1492,53594	3,66	43,17	1
0,0000	0	0,00006544	3,00	2	1192,49431	2,27	29,86	0

0,0000	0	0,0004891	2,89	2	1508,52995	3,03	31,58	1
0,0182	0,001	0,001126	2,69	2	1512,62065	2,70	34,86	1
0,0000	0,001	0,002779	2,60	2	1668,72392	3,73	30,00	2
0,0000	0,003	0,02093	1,95	2	1272,46001	1,63	32,29	0
0,0000	0,005	0,02805	2,70	3	1764,68387	2,80	25,84	2

# AAs	MW [kDa]	calc. pI
730	78,5	6,38

ΔCn	q-Value	PEP	XCorr	Charge	MH+ [Da]	ΔM [ppm]	RT [min]	# Missed Cleavages
0,0000	0	0,007226	3,39	2	1940,75383	5,04	73,73	0
0,0000	0	0,003986	1,91	3	1860,78714	5,07	64,05	0
0,0000	0,009	0,1429	1,41	2	1136,45891	4,53	66,45	0

# AAs	MW [kDa]	calc. pI
478	51,1	5,60

ΔCn	q-Value	PEP	XCorr	Charge	MH+ [Da]	ΔM [ppm]	RT [min]	# Missed Cleavages
0,0000	0	0,0004938	4,69	2	1841,80644	5,10	60,19	1
0,0000	0	0,0006005	3,71	3	1997,90366	2,75	52,69	2
0,0000	0	0,006039	3,57	2	1761,83440	2,09	54,30	1

# AAs	MW [kDa]	calc. pI
990	108,7	5,36

ΔCn	q-Value	PEP	XCorr	Charge	MH+ [Da]	ΔM [ppm]	RT [min]	# Missed Cleavages
0,0000	0	0,002858	3,62	2	1412,56816	2,85	38,69	1
0,0000	0	0,003099	2,34	2	1176,49858	1,61	38,92	0
0,0000	0,001	0,03315	3,43	2	1256,46745	3,53	44,27	0
0,0000	0,002	0,03821	2,53	2	1428,56194	2,02	27,08	1
0,0000	0,003	0,08073	2,99	3	1748,68888	2,78	34,09	2
0,0000	0,009	0,136	2,29	2	1877,70586	2,33	38,13	2

# AAs	MW [kDa]	calc. pI
730	78,5	6,38

ΔCn	q-Value	PEP	XCorr	Charge	MH+ [Da]	ΔM [ppm]	RT [min]	# Missed Cleavages
0,0000	0	0,000001034	2,86	2	1860,78716	5,08	68,38	0
0,0000	0	0,001696	2,17	2	1733,69402	4,97	61,50	0
0,0000	0	0,0001205	1,91	2	1187,54436	2,28	30,23	1
0,0000	0,001	0,003115	2,36	2	1267,51103	2,41	34,37	1
0,0000	0,003	0,02469	2,40	2	1940,75395	5,11	73,71	0
0,0000	0,007	0,07586	1,75	2	1136,45732	3,13	66,57	0

# AAs	MW [kDa]	calc. pI
478	51,1	5,60

ΔCn	q-Value	PEP	XCorr	Charge	MH+ [Da]	ΔM [ppm]	RT [min]	# Missed Cleavages
0,0000	0	0,000001233	4,99	2	1841,80559	4,63	60,78	1
0,0025	0	0,000001269	3,99	2	1761,83611	3,06	54,07	1
0,0000	0	2,175E-08	3,93	3	1997,90604	3,94	52,56	2

# AAs	MW [kDa]	calc. pI
990	108,7	5,36

ΔCn	q-Value	PEP	XCorr	Charge	MH+ [Da]	ΔM [ppm]	RT [min]	# Missed Cleavages
0,0000	0	0,000001046	3,98	2	1412,56841	3,02	38,75	1
0,0000	0	0,0005805	3,86	2	1256,46758	3,62	44,22	0
0,0000	0	9,888E-07	3,81	2	1492,53569	3,50	43,40	1
0,0000	0	0,0003444	3,78	2	1428,56182	1,93	29,91	1
0,0000	0	0,000002533	3,70	2	1508,52971	2,86	33,91	1
0,0000	0	0,00001159	3,29	2	1668,72087	1,91	30,68	2
0,0000	0	0,000003327	2,98	2	1348,59453	1,34	26,15	1
0,0000	0	0,00002493	2,80	2	1176,49980	2,64	39,00	0
0,0000	0	0,00009342	2,78	2	1512,62078	2,78	35,32	1
0,0000	0	0,001267	2,44	2	1192,49419	2,16	29,09	0
0,0000	0	0,0004907	1,71	3	1748,68833	2,46	35,28	2
0,0000	0,001	0,006498	2,94	2	1877,70635	2,59	39,78	2
0,0000	0,001	0,01192	2,79	2	1272,46062	2,11	32,13	0
0,0077	0,001	0,002234	2,57	2	1592,58684	2,47	39,97	1
0,0000	0,001	0,01203	2,12	2	1764,68083	1,07	25,84	2
0,0000	0,001	0,002954	1,92	2	1813,73393	2,14	28,07	2

0,0000	0,003	0,02919	1,85	2	1528,61601	2,96	26,63	1
0,0446	0,006	0,06709	1,93	2	1797,74077	3,13	35,97	2

# AAs	MW [kDa]	calc. pI
730	78,5	6,38

ΔCn	q-Value	PEP	XCorr	Charge	MH+ [Da]	ΔM [ppm]	RT [min]	# Missed Cleavages
0,0000	0	0,003691	3,00	2	1347,47722	2,16	34,93	1
0,0000	0	0,001617	2,86	2	1267,51091	2,31	34,46	1
0,0000	0	0,005526	2,47	2	1136,45598	1,95	66,43	0
0,0000	0,001	0,01081	2,36	2	1733,69402	4,97	61,63	0
0,0000	0,001	0,01268	1,91	2	1187,54350	1,56	30,14	1

# AAs	MW [kDa]	calc. pI
478	51,1	5,60

ΔCn	q-Value	PEP	XCorr	Charge	MH+ [Da]	ΔM [ppm]	RT [min]	# Missed Cleavages
0,0000	0	5,413E-08	5,06	2	1841,80254	2,98	60,30	1
0,0000	0	1,453E-08	3,95	3	1997,90384	2,84	52,78	2
0,0000	0	0,0000317	3,94	2	1761,83501	2,43	54,08	1

# AAs	MW [kDa]	calc. pI
990	108,7	5,36

ΔCn	q-Value	PEP	XCorr	Charge	MH+ [Da]	ΔM [ppm]	RT [min]	# Missed Cleavages
0,0000	0	0,000003151	3,74	2	1412,56731	2,24	39,11	1
0,0000	0	0,00002078	3,64	2	1492,53496	3,01	43,27	1
0,0000	0	0,0004442	3,51	2	1256,46623	2,56	44,45	0

0,0000	0	0,0007498	3,27	2	1877,70647	2,66	38,51	2
0,0000	0	0,002041	3,20	2	1428,56218	2,19	27,78	1
0,0000	0	0,0001105	3,05	2	1508,52910	2,46	31,64	1
0,0000	0	0,000114	2,87	2	1176,49822	1,30	40,04	0
0,0000	0	0,00242	2,85	2	1748,68962	3,20	34,92	2
0,0000	0	0,0001105	2,64	2	1512,61931	1,81	35,38	1
0,0000	0	0,002701	2,37	2	1348,59624	2,60	26,41	1
0,0000	0	0,0003466	2,03	2	1797,73931	2,32	35,91	2
0,0000	0,001	0,01293	2,03	2	1893,70049	2,16	29,01	2
0,0000	0,001	0,009618	1,93	2	1764,68120	1,28	26,11	2
0,0000	0,001	0,008109	1,37	2	1175,52324	2,32	28,02	1
0,0000	0,002	0,02078	1,56	2	1528,61553	2,64	26,30	1
0,0000	0,005	0,05862	2,20	2	1272,46001	1,63	32,48	0
0,0000	0,005	0,063	1,80	2	1592,58586	1,86	40,30	1

s. *Eukaryot Cell* 1(1):85-94

s. *Fungal Genet Biol* 23(3):288-99